NAVAL POSTGRADUATE SCHOOL
Monterey, California

THESIS

EXPERIMENTAL STUDIES OF APPLICATIONS OF TIME–REVERSAL ACOUSTICS TO NON-COHERENT UNDERWATER COMMUNICATIONS

by

Michael Gerhard Heinemann

March 2000

Thesis Advisor: Andrés Larraza
Co-Advisor: Kevin B. Smith

Approved for public release; distribution is unlimited.

REPORT DOCUMENTATION PAGE

Form Approved OMB No. 0704-0188

1. AGENCY USE ONLY *(Leave blank)*	2. REPORT DATE	3. REPORT TYPE AND DATES COVERED
	March 2000	Master's Thesis

4. TITLE AND SUBTITLE

Experimental studies of applications of time-reversal acoustics to non-coherent underwater communications

5. FUNDING NUMBERS

6. AUTHOR(S)

Heinemann, Michael.

7. PERFORMING ORGANIZATION NAME(S) AND ADDRESS(ES)
Naval Postgraduate School
Monterey CA 93943-5000

8. PERFORMING ORGANIZATION REPORT NUMBER

9. SPONSORING/MONITORING AGENCY NAME(S) AND ADDRESS(ES)

10. SPONSORING/MONITORING AGENCY REPORT NUMBER

11. SUPPLEMENTARY NOTES The views expressed in this thesis are those of the author and do not reflect the official policy or position of the Department of Defense or the U.S. Government.

12a. DISTRIBUTION/AVAILABILITY STATEMENT
Approved for public release; distribution is unlimited.

12b. DISTRIBUTION CODE

13. ABSTRACT *(maximum 200 words)*

The most difficult problem in shallow underwater acoustic communications is considered to be the time-varying multipath propagation because it impacts negatively on data rates. Computationally intensive and complex signal processing algorithms are required to compensate for symbol overlapping. This thesis presents results of a tank scale experiment to test Time-Reversal Acoustics (TRA) approach for high data rate binary transmissions. TRA can environmentally adapt the acoustic propagation effects of a complex medium. Our results show the suitability of the TRA approach in underwater acoustic communications. The results also show good focusing properties at an intended target location. The focal region extends over a few wavelengths, outside of which scrambling of the message occurs, offering natural encryption. Range shifts of the focal region could be achieved by frequency shifting. We found that the time focusing is aperture–size independent, but the spatial focusing is aperture–size dependent. Overall, we showed that our algorithm can accomplish a fast, secure, and stable communication scheme with low computational complexity.

14. SUBJECT TERMS:

Time reversal acoustics, Acoustic communications, Acoustic signal processing

15. NUMBER OF PAGES 71

16. PRICE CODE

17. SECURITY CLASSIFICATION OF REPORT	18. SECURITY CLASSIFICATION OF THIS PAGE	19. SECURITY CLASSIFICATION OF ABSTRACT	20. LIMITATION OF ABSTRACT
Unclassified	Unclassified	Unclassified	UL

NSN 7540-01-280-5500

Standard Form 298 (Rev. 2-89)
Prescribed by ANSI Std. 239-18 298-102

Approved for public release; distribution is unlimited.

EXPERIMENTAL STUDIES OF APPLICATIONS OF TIME–REVERSAL ACOUSTICS TO NON-COHERENT UNDERWATER COMMUNICATIONS

Michael Gerhard Heinemann
Kapitänleutnant, German Navy
Diploma, University of German Armed Forces, Munich, 1992

Submitted in partial fulfillment
of the requirements for the degrees of

MASTER OF SCIENCE IN ENGINEERING ACOUSTICS
AND
MASTER OF SCIENCE IN APPLIED PHYSICS
from the
NAVAL POSTGRADUATE SCHOOL
March 2000

Author: Michael Heinemann
Michael Gerhard Heinemann

Approved by:
Andrés Larraza, Thesis Advisor

Kevin B. Smith, Thesis Co-Advisor

Kevin B. Smith, Chairman
Engineering Acoustics Academic Committee

William B. Maier, Chairman
Department of Physics

ABSTRACT

The most difficult problem in shallow underwater acoustic communications is considered to be the time-varying multipath propagation because it impacts negatively on data rates. Computationally intensive and complex signal processing algorithms are required to compensate for symbol overlapping. This thesis presents results of a tank scale experiment to test Time-Reversal Acoustics (TRA) approach for high data rate binary transmissions. TRA can environmentally adapt the acoustic propagation effects of a complex medium. Our results show the suitability of the TRA approach in underwater acoustic communications. The results also show good focusing properties at an intended target location. The focal region extends over a few wavelengths, outside of which scrambling of the message occurs, offering natural encryption. Range shifts of the focal region could be achieved by frequency shifting. We found that the time focusing is aperture–size independent, but the spatial focusing is aperture–size dependent. Overall, we showed that our algorithm can accomplish a fast, secure, and stable communication scheme with low computational complexity.

TABLE OF CONTENTS

ACKNOWLEDGEMENTS

I wish to give recognition to:

My wife Kathrin for her love and patience.

To Andrés Larraza, his enthusiasm and passion for physics is nothing short of contagious.

To Kevin Smith, for valuable comments.

To members of the physics technical support team here at the Naval Postgraduate School:

Gary Beck

Eric Conner

David Grooms

George Jaksha

Donald Snyder

To these men, I am much indebted, their countless hours of support were instrumental in the creation of the apparatus and the success of this thesis.

Michael Heinemann

I. INTRODUCTION

For underwater acoustic propagation in shallow water environments, a narrow–band pulse generated by a point–like source spreads because of multi-path propagation due to reflections at the surface and at the bottom of the ocean or refractions within the interior. Each propagation path takes a different time, so that the transmitted pulse gives rise to multiple copies, not equally spaced in time, arriving at a receiver (Fig. 1.1). The strong signal degradation due to the multipath propagation is further enhanced by high spatial and temporal variability of the channel conditions that exist in a typical underwater acoustic channel in shallow water environments.

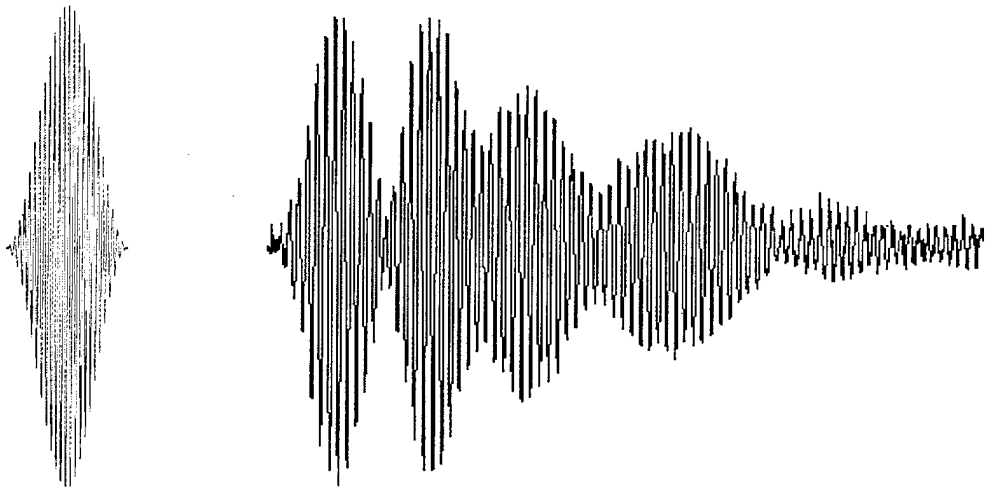

transmitted signal received signal

Figure 1.1. Example of transmitted and received signal in the multipath propagation environment of a rectangular waveguide. The time-scale for both signals is the same.

In a communication link, the signal degradation due to multipath spreading

causes Inter-symbol Interference (ISI) which is the interference between symbols due to multiple arrivals of each transmitted symbol. For example, in a shallow water channel a multipath spread of 100 ms with 1000 symbols per second, the ISI extends to over 100 symbols. Also, as long propagation times decrease data throughput, available bandwidth is severely limited by transmission loss, which increases both in frequency and in range.

A novel technique called Time-Reversal Acoustics (TRA) can environmentally adapt the acoustic propagation effects of a complex medium in order to focus energy at a particular target range and depth. Additionally, estimates show that TRA focusing can be done at useful ranges (30 km) and over reasonable time scales (30 min) without updating the time-reversed signal under certain conditions, as shown by Kuperman et al., (1998) in an ocean experiment using 445 Hz frequency signals. The TRA technique consists of digitizing the analog signal received by, say, a microphone or a hydrophone, time reversing it, and retransmitting it from a co–located source. If a wide-aperture array of receivers/transmitters is used, the time-reversed signal back at the point–like source is focused in time and space. For a small–aperture array, while the time–reversed signal back at the point–like source does not focus well in space, it still exhibits near–optimal focusing in time.

Because the path back from the array to the original source location is reciprocally identical (barring significant currents or other features which degrade reciprocity), the mode group speeds are also identical. Therefore, all of the modes arrive back at the original source location at the same time and add up

constructively. This generates both a temporal and spatial (range and depth) focusing of the propagating field. Thus, using TRA the multipath structure is eliminated because all of the propagation paths add coherently at the source location, which results in a reduced ISI of the communication link. Furthermore, due to spatial and temporal focusing there is a strong enhancement of the field at the focus location, which allows us to increase bandwidth and the transmission range. Also, because the spatial extent of the focus is a few wavelengths of sound, TRA possesses natural encryption for points other than the intended target.

An important step toward useful naval and commercial applications of TRA is to fully explore the capabilities and limits. This exploration, often repetitive in nature, is most cost effectively done in tank-scale experiments, and supplemented with numerical simulations.

The properties of time-reversal acoustics suggest a potential application in the field of non-coherent acoustic communications. This has previously been suggested by Jackson and Dawling (1991) and Kuperman et al. (1998). "Non-coherent" in this sense is meant to imply that no phase information will be transmitted in the communication signal but instead an energy detector method will be used. A novel communications scheme has been suggested by Abrantes et al. (1999) and Smith et al. (1999), which employs both the temporal and spatial focusing properties of TRA. In this scheme, two source/receiver systems, **A** and **B**, are used to communicate with one another. A set of distinct signals representing binary bits is agreed upon and known by the **A** and **B** systems.

Each signal should have roughly the same temporal resolution. A simple example would be multiple broadband signals with identical bandwidth, Hanning window source spectra, and center frequencies separated by half the bandwidth (allowing for null detection between adjacent signals). The total number of signals within the set is then limited primarily by the bandwidth of the system. For this example, assume that there are four distinct signals (bits) within the set defining a 4-bit character (giving values from 0-15). The communications link is achieved when a single element of **A** transmits each signal to **B** with sufficient time between transmissions for all multipath structure to arrive. This provides **B** with the transfer function of the environment for those signals. Then **B** has the ability to transmit binary information to **A** by building 4-bit "symbols" out of the time-reversed signals. In addition, the transmission of subsequent symbols can overlap each other significantly. The criterion for the delay between subsequent symbol transmissions is the temporal resolution of the focus back at **A**. For example, if the signals originally transmitted by **A** have a nominal temporal resolution of 10 msec, then **B** is able to transmit the 4-bit symbols at a nominal rate of 100 symbols/sec. Furthermore, recall that these focused signals arriving back at **A** have an improved SNR. Now consider that multiple elements in **A** each uniquely transmit the communication signals. Depending upon the spatial focusing properties of the time-reversed signals, multiple symbols may be transmitted from **B** to focus at different locations along **A**. Thus for a full transmission bandwidth of 1 kHz and a pulse bandwidth of 200 Hz, this scheme can provide a rate of 2,000 bits/s. This is comparable to current rates with the

added benefits of longer range due to energy focusing and covert coding due to the inherent scrambling induced by the environment at points other than the intended receiver.

The aim of this thesis is to establish an experimental study for the results found in previous simulations and to provide further knowledge about the relation of window size versus focal region size. Also the practicality of the method in underwater acoustic communications will be shown.

The organization of this thesis is as follows. In Chapter II, we describe the theory for TRA. Chapter III deals with the description of the apparatus. Chapter IV gives a description of the experiment and the definition of the symbols. Chapter V presents the results of different TRA measurements and the conclusions.

THIS PAGE IS INTENTIONALLY LEFT BLANK

II. TIME REVERSAL ACOUSTICS THEORY

This chapter presents an overview of time-reversal acoustics (TRA) theory. We concentrate here on the pulse excitation because of the relevance it bears with our experiment. Also we discuss the focal region properties and the issues of moving communications partners.

A. PULSE EXCITATION

In the following we give an overview of the theory for pulse excitation as described in Kuperman et al. (1998). For the geometry as shown in Fig. 2.1 we have for the jth element of the receiving array, consisting of a total of J elements, the following time-domain signal

$$P(R,z_j,t) = \int G_\omega(R,z_j,z_s)S(\omega)e^{-i\omega t}d\omega \qquad (2.1)$$

Here $P(R,z_j,t)$ is the pressure field as seen by the jth array element at range R, depth z_j and time t. $G_\omega(R,z_j,z_s)$ denotes the transfer function of the environment at the position of the jth element of the receiving array due to a point a point source at range r=0 and depth z=z_s and $S(\omega)$ is the initial pulse transmitted at frequency ω. This expression includes all effects of the waveguide environment, such as time elongation of the pulse due to multipath propagation. For convenience we set the time origin such that $P(R,z_j,t) = 0$ outside the time-interval $[0,\tau]$, where τ is a time greater than the length of the time-stretched signal. The time-reversed signal that will be retransmitted from the jth element will

then be $P(R,z_j,T-t)$, where $T>2\tau$ is an arbitrary point in time. This condition is imposed by causality. The signal has to be completely received before it can be time reversed. Note that the time reversal in the time-domain is the equivalent to the phase conjugation in the frequency-domain. The time-reversed pressure field can be written as

$$\begin{aligned} P(R,z_j,T-t) &= \int G_\omega(R,z_j,z_s)S(\omega)e^{-i\omega(T-t)}d\omega \\ &= \int [G^*_\omega(R,z_j,z_s)e^{i\omega T}S^*(\omega)]e^{-i\omega t}d\omega \end{aligned} \tag{2.2}$$

Thereby the sign of the integration variable ω has been reversed and the conjugate symmetry of the frequency-domain Green's function and initial pulse has been used. * denotes the complex conjugate. The bracketed expression in Eq. (2.2) is the Fourier transform of the signal received by the j^{th} array element after time reversal and time-delay. Further we find that this expression is the frequency-domain representation of the retransmitted signal. We can therefore use Fourier synthesis to obtain the time-domain representation of the field produced. The resulting acoustic field satisfies the wave equation

$$\nabla^2 P_{tr}(r,z) + k^2(z)P_{tr}(r,z) = \sum_{j=1}^{J}\delta(z-z_j)G^*_\omega(R,z_j,z_s) \tag{2.3}$$

where $k(z)$ is the depth dependent wave number.

For a vertical line of discrete sources we find the solution of Eq. (2.3) - using Green's function theory - to be

$$P_{tr}(r,z,\omega) = \sum_{j=1}^{J}\int G_\omega(r,z,z_j)G^*_\omega(R,z_j,z_s)e^{i\omega T}S^*(\omega)e^{-i\omega t}d\omega \tag{2.4}$$

Equation (2.4) can be used to show that the time reversal process produces focusing in time as well as in space. The focusing in time occurs because a form of matched filtering is done.

To show this, we examine the time revered field at the focus point, meaning we set in Eq. (2.4) $r = R,\ z = z_s$. If we neglect the density gradients, reciprocity allows the interchange $G_\omega(R, z_s, z_j) = G_\omega(R, z_j, z_s)$ (Jensen et al. (1993)). Using the time-domain representation of the Green's function and initial pulse the time-domain equivalent of Eq. (2.4) becomes (Kuperman et al. (1998))

$$P(r,z,t) = \frac{1}{(2\pi)^2} \int \sum_{j=1}^{J} \left[\int G_{t'+t''}(R, z_j, z_s) \times G_{t'}(R, z_j, z_s) dt' \right] S(t'' - t + T) dt'' \quad (2.5)$$

Note that the Green's function is correlated with itself, which is a matched filtering operation. The time elongation due to multipath propagation is reduced, hence we focus in time. The sum over all elements form a spatial matched filtering, that is to say we focus also in space.

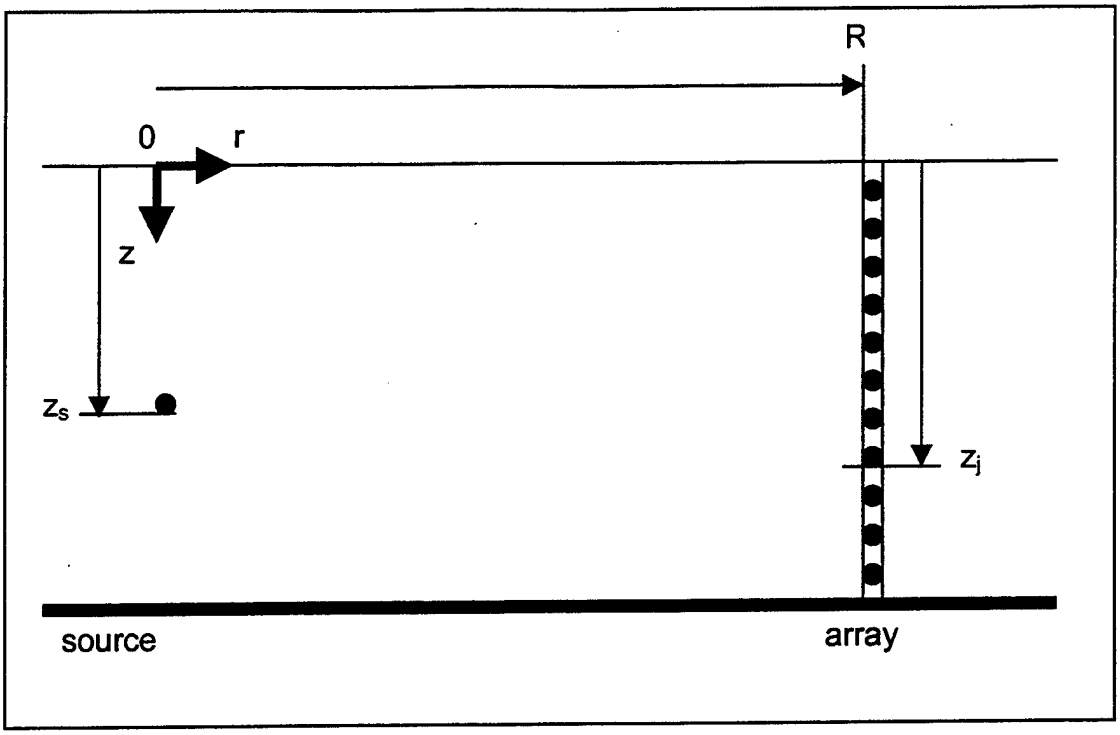

Figure 2.1. The geometry of the experiment as it is used in the description of the time reversal theory.

B. FOCAL REGION PROPERTIES

The primary factors influencing the time reversal focusing are the size of the time window chosen and the degradation of the signal due to the environment. The later can be divided into static and dynamic categories. The static category includes propagation and array structure effects. The dynamic one includes the time-varying environmental effects (Kuperman et al., 1998).

We can write the field at the array in the general form

$$P_{tr}(r,z,\omega) = \sum_{j=1}^{J} G_2(r,z;0,z_j) G_1^*(0,z_j;R,z_s) \tag{2.6}$$

Thereby $G_1(0,z_j;R,z_s)$ is the Green's function describing the propagation form source to array and $G_2(r,z;0,z_j)$ the one describing the propagation from array to any field point. The subscripts 1 and 2 allow for a changing environment within the two transmissions. However, we assume that during each transmission the environment is "frozen".

1. Time reversal focusing in static environment

We will examine the time reversal focusing in static environments by considering a general nonuniform, nonadiabatic waveguide. First we will derive the "ideal" case and then identify the degrading factors. For simplification we consider only vertical arrays. We assume small regions to be range-independent but larger regions to be range-dependent.

The Green's function is approximated using range-independent normal modes. The Green's function near the source can therefore be written as (Kuperman et al., (1998))

$$G_\omega(r,z;R,z_s)=\sum_n \frac{a_n(z_s)u_n(R,z)}{\sqrt{k_n(R)|r-R|}}e^{ik_n(R)|r-R|} \quad . \tag{2.7}$$

Similarly the Green's function near the array is

$$G_{ij}(0,z_j;R,z_s)=\sum_n \frac{b_n(z_s)u_n(0,z)}{\sqrt{k_n(0)R}}e^{ik_n(0)R} \quad . \tag{2.8}$$

The modal eigenfunctions are denoted as $u_n(R,z)$ and $u_n(0,z_j)$, respectively. The corresponding eigenvalues are $k_n(R)$ and $k_n(0)$. These Green's functions do not carry the subscripts 1 and 2, because we here look at the time-invariant case. The mode amplitudes for the near source and near array expressions are (Kuperman et al., (1998))

$$a_n(z_s)=\frac{ie^{-i\frac{\pi}{4}}}{\sqrt{8\pi\rho(z_s)}}u_n(R,z_s) \tag{2.9a}$$

and

$$b_m(z)=\sum_n U_{mn}a_n(z)\,. \tag{2.9b}$$

ρ is the density of the medium.

For convenience we assume that there are the same number of modes excited at both locations. This leads to U_{mn} being a square matrix (Kuperman et al., (1998)). The matrix U_{mn} includes any mode coupling due to the range-dependence and is defined independent of the source depth. Also U_{mn} is unitary,

as far as the absorption loss in the water column and into the bottom can be neglected.

The field produced by the array is described by Eq. (2.6), if we do not allow for a time-variant environment. The Green's function for the propagation from the j[th] element to any field point therefore, in terms of mode amplitudes, becomes

$$G_\omega(r,z;0,z_j) = \frac{\rho(z)}{\rho(z_j)} \sum_n \frac{c_n(z) u_n(0,z_j)}{\sqrt{k_n(0) r}} e^{ik_n(0)R} \tag{2.10}$$

Where the mode amplitudes $c_n(z)$ are essentially the same as $b_n(z)$, but with the source range shifted by $r - R$

$$c_m(z) = \sum_n U_{mn} a_n(z) e^{ik_n(R)(r-R)} \tag{2.11}$$

Putting everything together we get an expression for the time-reversed field in a range-dependent waveguide (Kuperman et al., (1998))

$$P_{tr}(r,z,\omega) = \frac{\rho(z)}{\sqrt{Rr}} \sum_{m,n} \frac{c_m(z) \Delta_{mn} b_n^*(z_s)}{\sqrt{k_m(0) k_n^*(0)}} e^{i\left[k_m(0) - k_n^*(0)\right]R} \tag{2.12}$$

Here Δ_{mn} is

$$\Delta_{mn} = \sum_{j=1}^{J} \frac{u_m(0,z_j) u_n(0,z_j)}{\rho(z_j)} \tag{2.13}$$

In the ideal case, the array spans the full water column and its elements have equal spacing d_a. In the bottom the amplitudes are negligible. In this case the sum over array elements in (2.13) approximately equals the orthogonality integral for modal eigenfunctions. For this case we get (Kuperman et al., (1998))

$$P_{tr}(r,z,\omega)=\frac{\rho(z)}{d_a\sqrt{Rr}}\sum_{m,n}Q_{mn}a_m(z)a_n^*(z_s)e^{ik_m(R)(r-R)} \tag{2.14}$$

where

$$Q_{mn}=\sum_l\frac{U_{lm}U_{ln}^*}{k_l(0)}e^{-2\mathrm{Im}(k_m(0))R} \quad . \tag{2.15}$$

The losses due to scattering and absorption are detrimental to time-reversal focusing because they attenuate higher-order modes, resulting in a blurrier focus than without loss. This blurring will increase with distance between source and array due to the strong range and mode number dependence of attenuation.

For the ideal case, that is no losses and unitary mode coupling matrix U_{mn}, we find

$$Q_{mn}=\frac{\delta_{mn}}{k_m(0)} \quad . \tag{2.16}$$

This leads to a time-reversal field for an ideal array in a lossless environment of the form (Kuperman et al., (1998))

$$P_{tr}(r,z,\omega)=\sum_n\frac{u_n(R,z)u_n(R,z_s)e^{ik_n(R)(r-R)}}{8\pi\rho(z_s)k_n(0)d_a\sqrt{Rr}} \tag{2.17}$$

Even though Eq. (2.17) represents the ideal case, it illustrates the properties of actual time-reversal arrays, as long as they are not too far from ideal. The independence of the focus region from the distance between source and array, as long as losses can be neglected, is one such property. This means

that only local environmental properties affect the focus region and that there is no range dependence.

The derivation above is essentially two-dimensional. If static out-of-plane scattering occurs, this will lead to degradation if one-dimensional arrays are used. However, this will not affect planar or spherical arrays.

2. Time reversal focusing in time-varying environments

In a real environment there occur changes in time due to surface and internal waves and sound speed profile changes. To discuss their influence on time reversal focusing it is convenient to decompose the Green's function into a coherent and an incoherent part (Kuperman et al., 1998),

$$G_\alpha(\vec{r},\vec{r}') = \overline{G}(\vec{r},\vec{r}') + \delta G_\alpha(\vec{r},\vec{r}') \ . \tag{2.18}$$

In Eq. (2.18), α is either 1 or 2, the subscripts as used before. The coherent part $\overline{G}(\vec{r},\vec{r}')$ is without subscript because it is unchanging. We assume that there is an uncorrelated change in the environment.

$$\left\langle \delta G_2(\vec{r}_d,\vec{r}_c)\delta G_1^*(\vec{r}_b,\vec{r}_a)\right\rangle = \left\langle \delta G_2(\vec{r}_d,\vec{r}_c)\delta G_1(\vec{r}_b,\vec{r}_a)\right\rangle = 0 \tag{2.19}$$

Where $\vec{r}_a,\vec{r}_b,\vec{r}_c$ and $\vec{r}_d$ are the vectors to arbitrary points in space. Using Eqs. (2.6), (2.18) and (2.19), we find the mean time-reversed field to be

$$\overline{P}_{tr}(r,z,\omega) = \sum_{j=1}^{J} \overline{G}\,(r,z;0,z_j)\overline{G}^*(0,z_j;R,z_s) \tag{2.20}$$

where $\bar{}$ denotes the averaged value and the subscript tr stands for time-reversed, and the variance of the field

$$\begin{aligned}&\overline{\left|P_{tr}(r,z,\omega)\right|^2}-\left|\overline{P}_{tr}(r,z,\omega)\right|^2\\&=\sum_{j=1}^{J}\sum_{j'=1}^{J}\left[\begin{array}{l}G\,(r,z;0,z_j)\overline{G}^*(0,z_j;R,z_s)K_{jj'}(R,z_s)\ldots\\+G\,(R,z_s;0,z_j)\overline{G}^*(R,z_s;0,z_{j'})K_{jj'}(r,z\,)+K_{jj'}(r,z\,)K_{jj'}(R,z_s)\end{array}\right]\end{aligned} \tag{2.21}$$

where

$$K_{jj'}(r,z)=\left\langle \delta G_\alpha(0,z_j;r,z)\delta G_\alpha^*(0,z_{j'};r,z)\right\rangle \quad . \tag{2.22}$$

The covariance $K_{jj'}(r,z)$ is proportional to the correlation between the incoherent field at the j^{th} and j'^{th} element of the array. We used reciprocity properties to get Eq. (2.20), allowing for interchange of the Green's function arguments, and stationarity, meaning that δG_1 and δG_2 have the same statistics.

Note that Eqs. (2.20) and (2.21) are general and include three-dimensional cases. They lead to the conclusion that the mean focus field can be obtained by using the coherent Green's function rather than the actual, random one. Further it is found that the field near the source is not fluctuating significantly.

3. Time reversal focusing range shifts

Song et al. (1998) stated that the sound field in an ocean environment is characterized by the existence of lines of maximum intensity $I(w,\vec{r})$ having a slope β. This slope is invariant for a particular group of modes.

$$\beta = \frac{r}{\omega}\left(\frac{\Delta\omega}{\Delta r}\right) = -\frac{d\left(\frac{1}{\mathrm{v}}\right)}{d\left(\frac{1}{\mathrm{u}}\right)} \tag{2.23}$$

Here v and u are the phase and group velocities characterizing the given mode group. It is further stated that β is an invariant because it is determined by the properties of the medium and the derivative in Eq. (2.23) averaged over the mode group of interest. The invariant property applies to the sound intensity, the phase velocity and the group delay. Therefore the invariant property holds for broadband pulses or multiple center frequency narrowband signals, provided that the mode shapes do not change significantly over the bandwidth.

Song et al. (1998) derived that a frequency shift leads to a shift of the focal range. The new focal range R' can be expressed relative to the old focal range as

$$R' = R\left(1-\frac{1}{\beta}\frac{\Delta\omega}{\omega}\right)^{-1} \cong R\left(1+\frac{1}{\beta}\frac{\Delta\omega}{\omega}\right) \tag{2.24}$$

For the case of a Pekeris waveguide with $\beta = 1$ this leads to a relation where an increase of the frequency by p percent leads directly to an increase in range of p percent.

It should be noted that Eq. (2.24) is an approximation in the sense that the frequency dependence of the mode amplitude is neglected. Also the expansion is only valid for a bounded group of modes for a given R and ω, and further multimode propagation was assumed in the derivation.

III. APPARATUS

In this chapter we describe the apparatus, instrumentation, and experimental techniques used to communicate in a shallow water environment using acoustic time-reversal techniques. The main components of the experiment were the computerized data generation and acquisition system with its two transducer arrays.

A. THE ACOUSTIC ENVIRONMENT

The experiment is conducted in a fiberglass coated wooden tank. The side-walls of the tank are covered by anechoic tiles to remove the influence of cross-range reflections. This tank simulates a shallow-water environment waveguide with infinite horizontal dimensions.

1. The Tank

The tank, shown in Fig. 3.1, is made of wooden plates of 18 mm thickness which are sideways reinforced every 65 cm. The inner dimensions are 15.32 m length, 1.17 m width and 1.20 m depth. For better sealing the wood is covered with a layer of fiberglass. The tank rests on a concrete floor on foundation level.

The Seawhisper^{TM} anechoic tile system made by Seaward International, Inc. is positioned 8 cm away from the tank-walls. Two tiles are aligned vertically covering a height of the wall of 28 cm. The material reduces the echo reflection

by about 25 dB in the frequency range between 20 kHz and 100 kHz at normal incidence. An echo reduction versus frequency plot is shown in Fig. 3.2. The tank acts therefore as a horizontally infinite waveguide with almost rigid bottom and pressure release surface.

On top of the tank sits a rail system on which two carts can move. The carts are able to carry equipment and hold the transducer arrays. One of them is driven by a step-motor, which is steered remotely from the computer system.

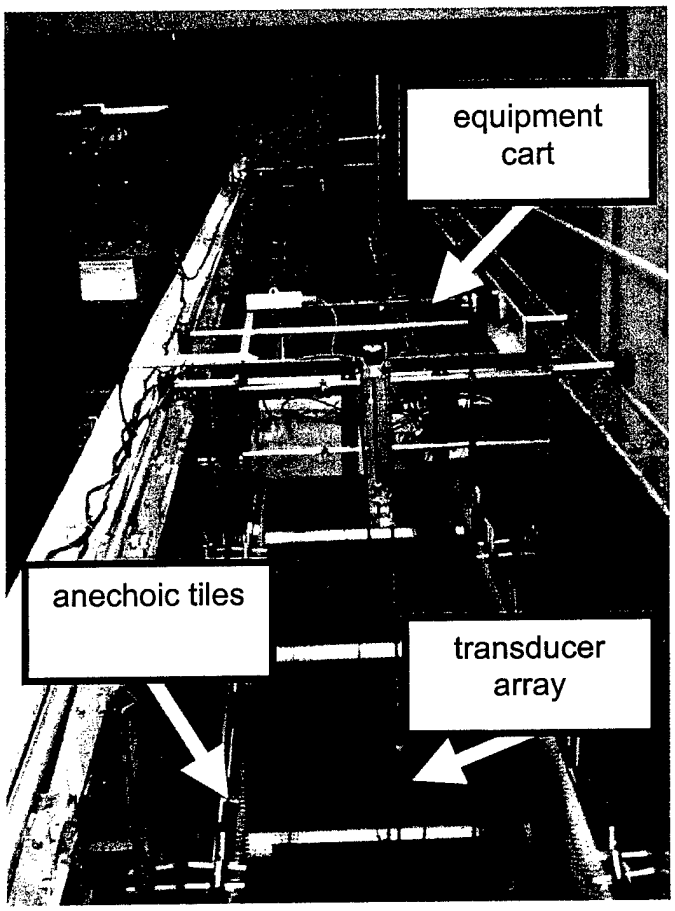

Figure 3.1. View from above one end of the tank. The tank has inner dimension of 15.32 m length, 1.17 m width and 1.20 m depth. The water level can be raised up to 28cm, the height of the anechoic material.

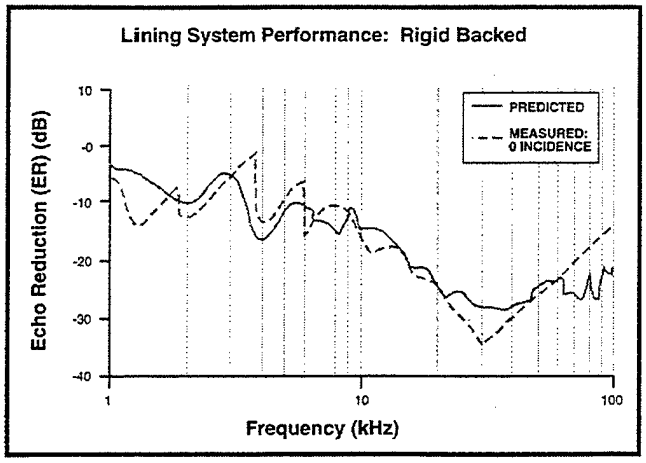

Figure 3.2. Echo reduction versus frequency plot for the Seawhisper™ anechoic tile system covering the side walls. (A&T Engineering Technologies, VECTOR Research Division)

2. The transducer arrays

The two transducer arrays, made by EDO Electronic-Ceramic Products, consist of ten cylindrical piezo-ceramic elements each (see Fig. 3.3). The elements are positioned with its vertical cylindrical axis within a PVC tube. The dimensions of the arrays are 38 mm diameter and 305 mm length.

The hoop mode frequency of all the elements is around 73 kHz. All elements by themselves in both arrays are horizontally omni-directional. The elements are all matched to one another very well as is shown in the calibration reports (EDO Corporation, Acoustic Division, September 30,1998).

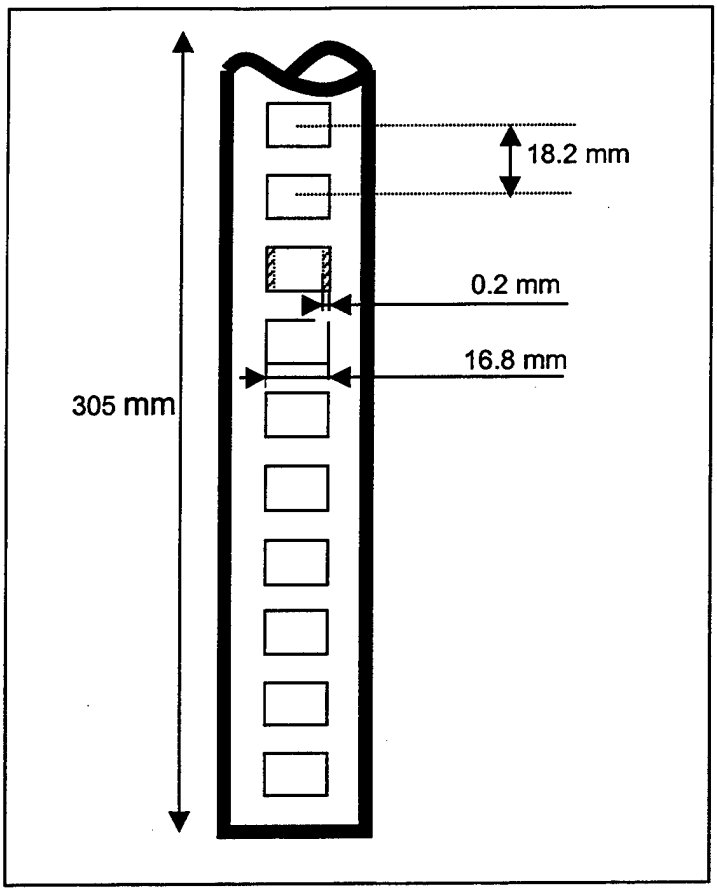

Figure 3.3. The design of the ten-element transducer arrays made by EDO Electro-Ceramic Products of dimensions 38 mm diameter and 305 mm length.

B. THE COMPUTERIZED DATA GENERATING AND ACQUISITION SYSTEM

The data acquisition and generation system is made by Gage Applied Sciences Inc. and is PC-based. It consist of eight CompuGen 1100 function generator cards and four dual channel CompuScope 512 oscilloscope cards for a total of eight input and eight output channels available.

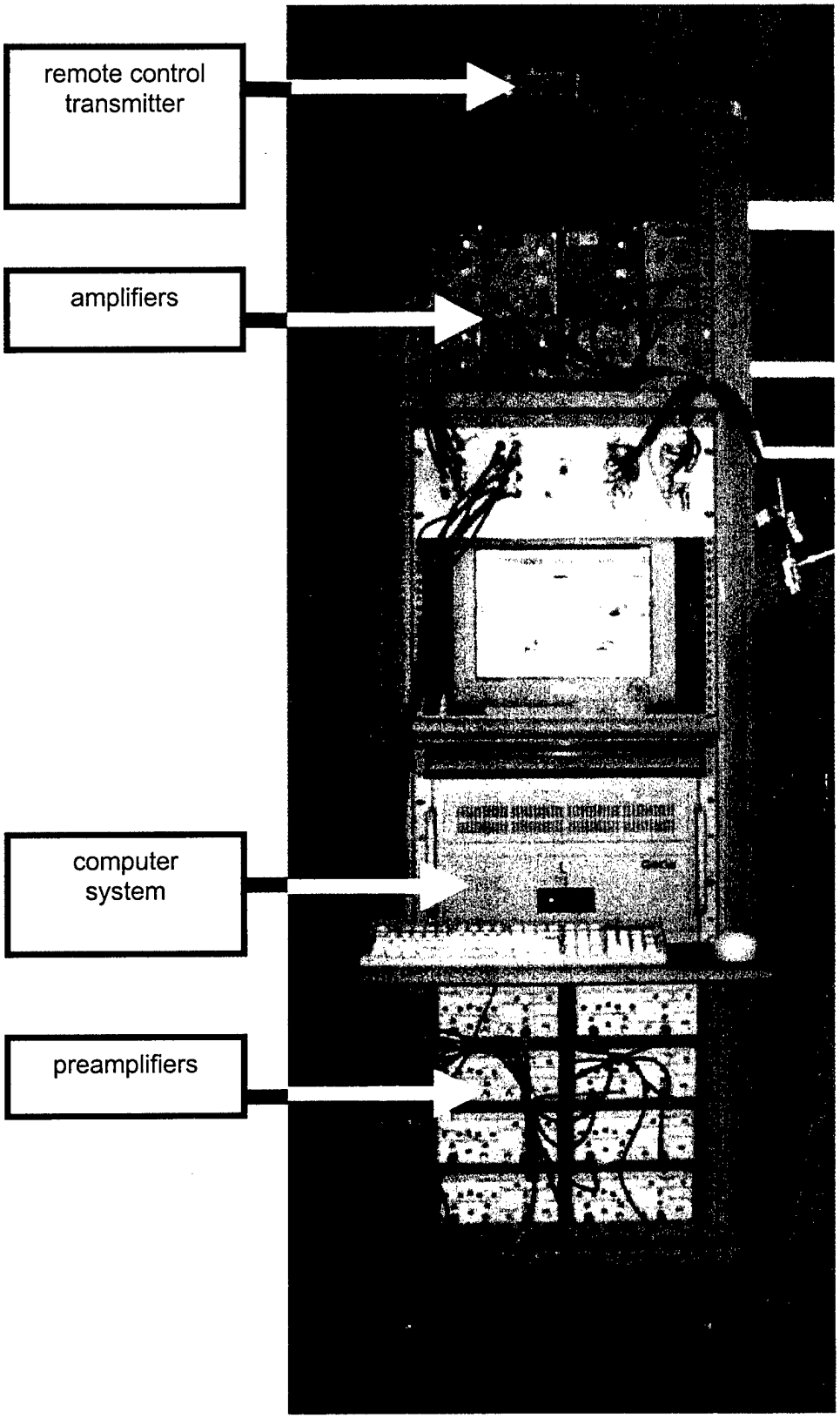

Figure 3.4. The computer system with the preamplifiers, the 8-channel-switch, the amplifiers and remote control transmitter.

1. The computer and operating system

The computer features a 266 MHz Pentium II CPU, 64 MB RAM, 6 GB hard-drive, 1 CD-ROM drive, 1 3.5" floppy disc, a VGA graphics card, a 15" monitor and a net card. The operating systems are DOS 7.0 and Windows 98.

2. The function generators

The function generation is done with CompuGen 1100 function generator cards. Among their key features are: up to 80 Msamples per second, 12-bit resolution and up to 16 Msample memory buffers (Gage Applied Sciences Inc., February 1998). Function generator card number one acts as master and the seven other cards act as slaves.

3. The oscilloscopes

The data capture is done with CompuScope 512 oscilloscope cards. Their key features are: up to 5 Msamples per second, 12-bit resolution and 2 MB memory. They have all features of Digital Storage Oscilloscopes (Gage Applied Sciences Inc., February 1998).

4. The software

The cards are addressed via two MEX-files from Gage Applied Sciences, which are called by MATLAB programs. The MATLAB software was written by the author to fit our special needs. It includes the key features definition of signals to be transmitted, editing of captured signals, including cutting, amplifying

and time-reversing, setting the parameters of and initializing the data system, data storing, visualization and analysis of the data. The software offers four graphical user interface windows, as shown in Fig. 3.5. The main window allows the experiment to run, while the two signal creation windows allow prepare signals to be prepared and messages to be used in the experiment. The remote control window allows changing the position of one equipment cart and both arrays in order to change the geometry of the experiment.

5. Amplifier

To amplify the output of the function generators we used a set of eight HP 467A amplifiers. This allowed us to amplify the signals up to ±20 V peak to peak.

6. Preamplifier

Pre-amplification of the received analog signals, before they were captured by the oscilloscope cards, was done with a set of eight Stanford SR560 preamplifiers. Preset 6dB/ocatve filtering of the incoming signals can be accomplished directly with the built-in filters.

7. Switch

To switch the eight outgoing and the eight incoming channels from a parallel (meaning amplifiers to transducer #1 and transducer #2 to preamplifiers) to a crosswise (meaning amplifiers to transducer #2 and transducer #1 to

preamplifiers) connection we used a relays switch arrangement, using a total of 8 relays (one per channel).

8. Remote Control Equipment

To remotely move the position of one equipment cart in range and the two transducer arrays in height, we used a radio transmitter set and stepping motors.

IV. EXPERIMENT DESCRIPTION

In this chapter we describe the experiments we conducted using TRA techniques as applied to underwater acoustic communications.

Using common procedures for calibration and testing, we found it best to use a frequency range between 50 kHz and 65 kHz. Below this range, the response of our system was weak, and electronic noise at 30 kHz and 35 kHz would yield a small signal-to-noise ratio (SNR); also switching the relays into the on position would cause 60 Hz noise. Above the frequency range of operation, the strong response at resonance (~73 kHz) overshadowed the response at other frequencies.

A. DEFINITION OF SYMBOLS

In the following we will use the expression symbol for a single pulse containing one, two, three or all four center-frequencies. A symbol thus contains information which can be related to a code. Four center-frequencies can be combined into 15 different ways, excluding the null symbol which contains no acoustic energy. For each combination we assigned a number between 1 and 15 as shown in Table 4.1.

SYMBOL NUMBER	1	2	3	4	5	6	7	8	9	10	11	12	13	14	15
Center-Frequency 1	x		x		x		x		x		x		x		x
Center-Frequency 2		x	x			x	x			x	x			x	x
Center-Frequency 3				x	x	x	x					x	x	x	x
Center-Frequency 4								x	x	x	x	x	x	x	x

Table 4.1. The center-frequencies used in each symbol.

B. RESOLUTION OF SYMBOLS

The four center frequencies we used are at 50 kHz, 55 kHz, 60 kHz and 65 kHz. The initial pulse transmissions used one single center frequency at a time. The pulses were created using different bandwidths, corresponding to different lengths in time. The pulses were then multiplied by a Hanning window, but we also used a rectangular and a Bartlett window during our testing.

1. The initial transmission

The initial transmission commonly was done in the parallel switch setting, meaning that transducer array #1 transmitted and transducer array #2 received. The resulting reception contained all the multipath propagation. We then selected a window that contained all the multipath propagation information to create the time reversed signal, making sure that the window size within one set of data was the same and that the relative position of the time windows at the first arrival was the same.

2. The messages

The operation described above resulted in time reversed signals which we used to build the messages containing various symbols. Usually we started with a message using the symbols '1-2-4-8-15'. The spacing between the symbols was varied. This allowed discrimination of the response of the single frequencies as well as the response of the combination of all of them. For further messages we could use the knowledge about the response to adjust the amplitudes between the center-frequencies relative to each other. The message we defined

in this way was sent with the crosswise switch setting, meaning that transducer array #2 transmitted and transducer array #1 received.

3. Bandwidth limit and spacing between symbols

We send the messages created as described above and checked whether we could resolve them by a matched filter approach and by a FFT approach. We did this for bandwidths of 10 kHz, 5 kHz, 4 kHz, 3 kHz, 2.5 kHz, 2 kHz, 1.5 kHz, and 1 kHz. The spacing between symbols was also varied from none to one symbol length.

C. FOCAL REGION SIZE

1. Full array

To determine the focal region size we used a single time-reversed signal rather than a symbol or a message. Starting at the range at which the time-reversed signal was received we decreased and increased the range by steps of 1 cm. The time-reversed signal was sent at each of the positions and the signal received was checked for time and spatial (in depth) focus. We increased/decreased the range until time-focus was not resolved.

2. Reduced number of elements

For an amplitude adjusted time-reversed signal with frequency 50 kHz and bandwidth 2000 Hz we used one, two and three element combinations to transmit the time reversed signal. We compared these receptions with the all-element array reception for the same signal. This comparison allowed us to determine the minimum number of elements that would still give good temporal and spatial focus.

D. FOCAL REGION STEERING IN RANGE

We shifted the frequencies of the time-reversed signals in order to focus at different ranges. These new time-reversed signals were transmitted as before, with the receiving transducer moved to the new expected focus location. Then we increased/decreased the range in steps of a wavelength in order to find the size of the new focal region and its center. The expected focal range was determined from Eq. (2.24), with a value of $\beta = 1.0$. This turned out to be a good starting point.

V. RESULTS

In this chapter we will describe and analyze the results of the experiments described in chapter IV.

A. RESOLUTION OF SYMBOLS

The resolution of symbols depends on the quality of the reception and the means used to resolve the frequency data they contain. We used two simple approaches. In the first we performed an FFT on each symbol separately. In the second approach we analyzed the symbols by match filtering the received signals with the individual initial signals at each center frequency.

1. Bandwidth and spacing limits using a FFT

The three quantities that determine data rates are inter-symbol spacing, bandwidth, and center frequency spacing. The bandwidth determines the time span of the symbol, and the frequency spacing determines the resolution of the information contained in a symbol. The inter-symbol spacing is mainly determined by the energy of the sidelobes at the focal point. The use of a Hanning window minimized the sidelobes allowing also for no spacing between the symbols. This is not the case for a rectangular window. Thus, under the condition of no symbol spacing, it is important to select frequency signals which give a reception that can be resolved in its frequency components. This condition was fulfilled for the center frequencies mentioned previously with a bandwidth of

2 kHz. Figure 5.1 shows a message with 2.5 kHz bandwidth, which is not resolvable and one with 2 kHz bandwidth, which is clearly resolvable. Note that because the center frequency spacing is 5 kHz, there exists a ratio of 5 to 2 for the center frequency spacing to the bandwidth.

We set the thresholds for accepting the signal after undergoing a FFT as a minimum of 6 dB difference between the lowest amplitude valid peak and the highest noise peak. Also we required that the valid peaks all lay within 9 dB of the highest amplitude within the symbol. We found these conditions necessary in order to have automation capability for analyzing the messages.

We also varied the spacing between symbols. The spacing was decreased from a full symbol length to no spacing at all. In Fig. 5.2a and Fig. 5.2b we show the FFT for a spacing of one symbol length and no spacing respectively .

In the rest of the analysis we will only use messages without symbol spacing, since this is the more desirable case in order to have high data rates. Also we will use Hanning window signals throughout.

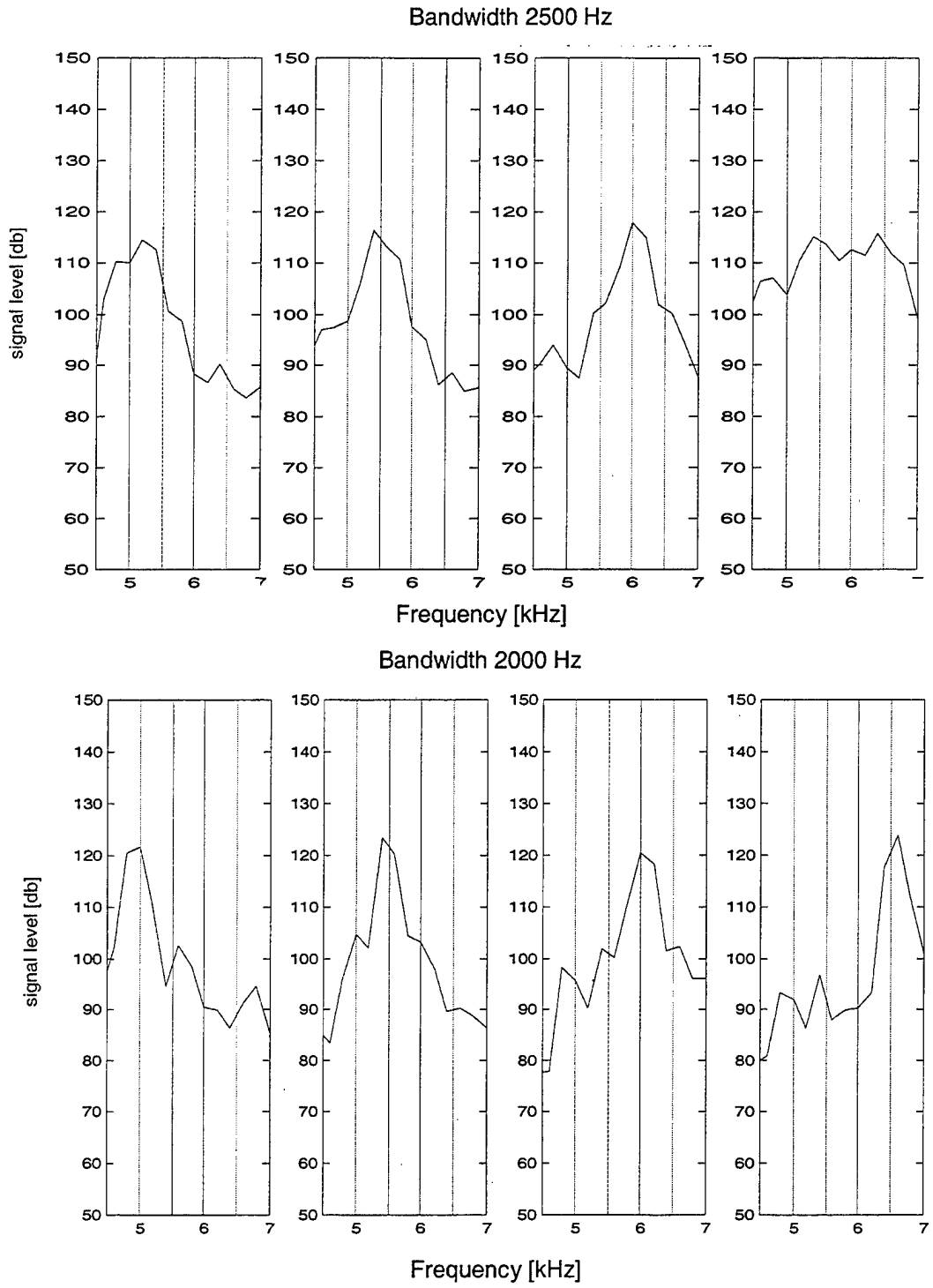

Figure 5.1 Two messages containing the symbols 1 - 2 - 4 – 8. The left message has a bandwidth of 2500 Hz and is not resolvable. The right message has a bandwidth of 2000 Hz and it is clearly resolvable.

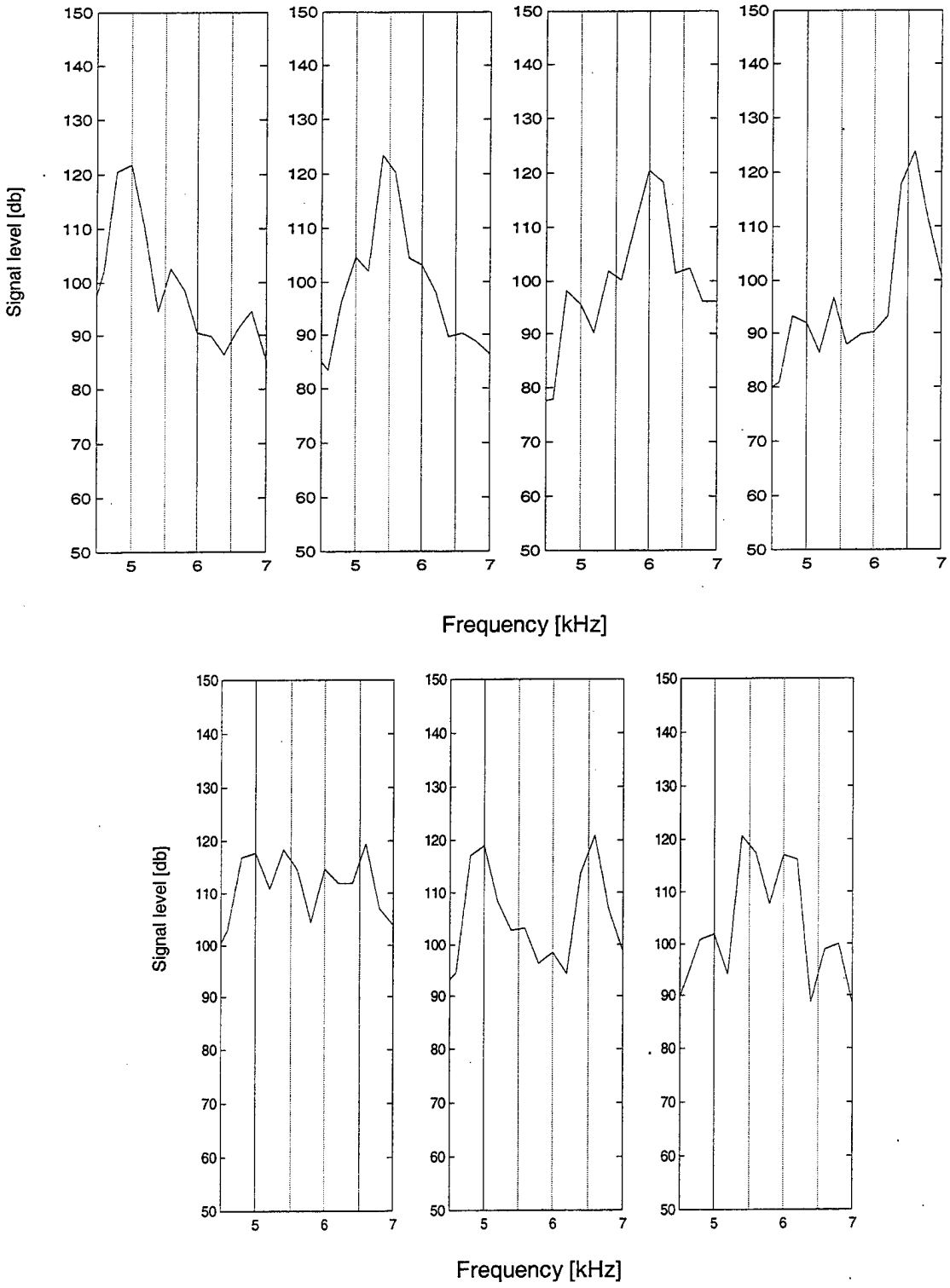

Figure 5.2.a Two messages with one symbol length spacing. The left message contains the symbols 1 - 2 - 4 - 8 and the right message the symbols 15 - 9 - 6.

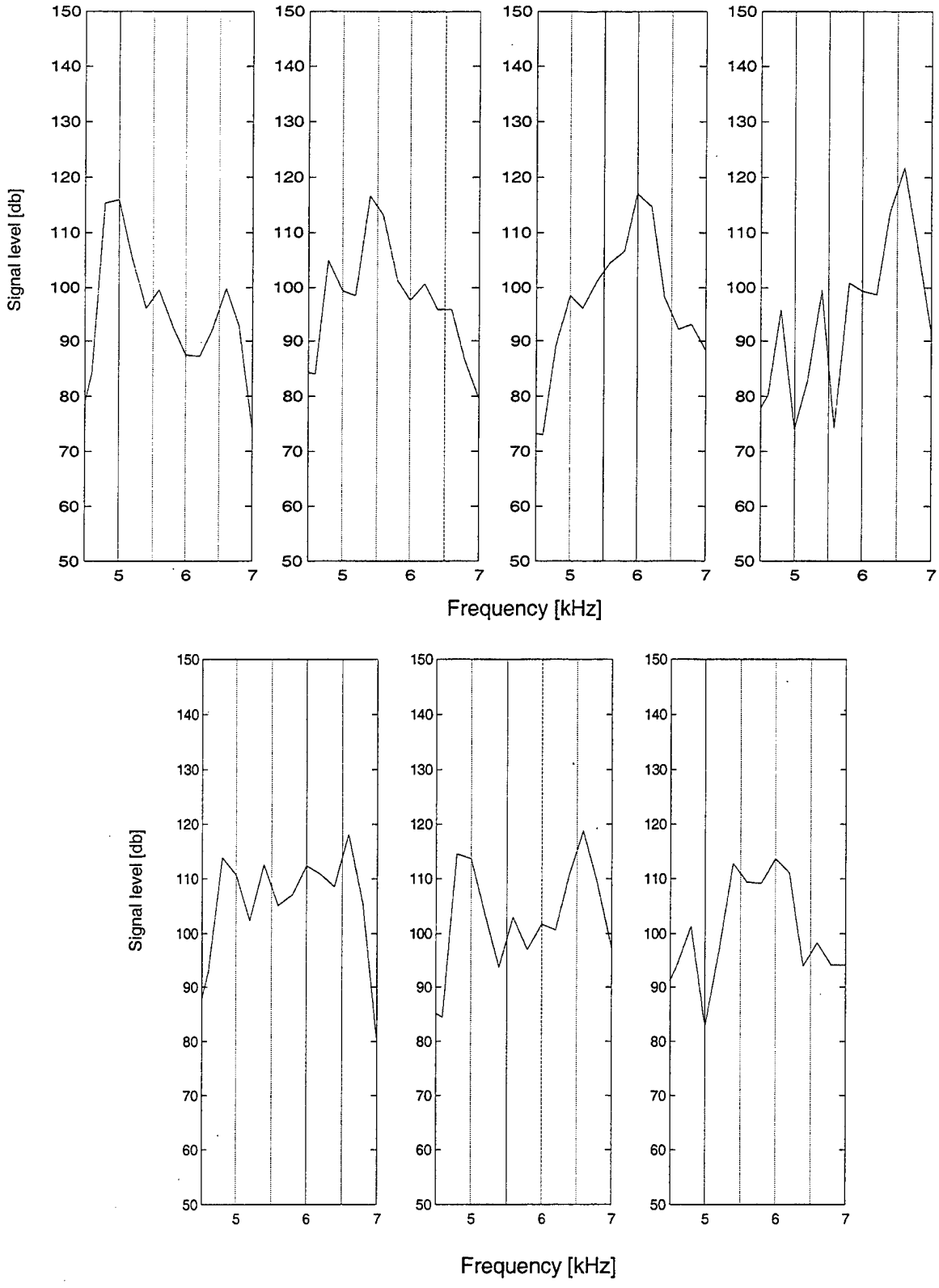

Figure 5.2.b Two messages with no spacing. The left message contains the symbols 1 - 2 - 4 - 8 and the right message the symbols 15 - 9 - 6.

2. Bandwidth limits using a Matched Filter

For a message containing Hanning window signals and having no spacing we found that there is a maximum bandwidth of 2500 Hz, when the received symbols were match filtered with the initial signals whose frequency spacing is 5 kHz. Therefore we find a ratio of 2 to 1 for center frequency spacing to bandwidth.

Our criteria for accepting a signal as resolvable is that the sidelobes must be less than half the amplitude of the main peaks. This criteria is based on the notion that when the sidelobes of two adjacent symbols are added, the symbol can still be resolved.

Figure 5.3 shows messages with 2.5 kHz and 3 kHz bandwidth. The 2.5 kHz bandwidth message barely meets our criteria, while the 3 kHz bandwidth messages does not.

The matched filter approach to resolve the symbols of the messages turned out to be the more desirable one, both because the resolvable bandwidth is larger and also because it is easier to apply. With the matched filter the frequency content of all symbols in a message is deciphered at once without having to define the time window for execution as it is done with the FFT approach.

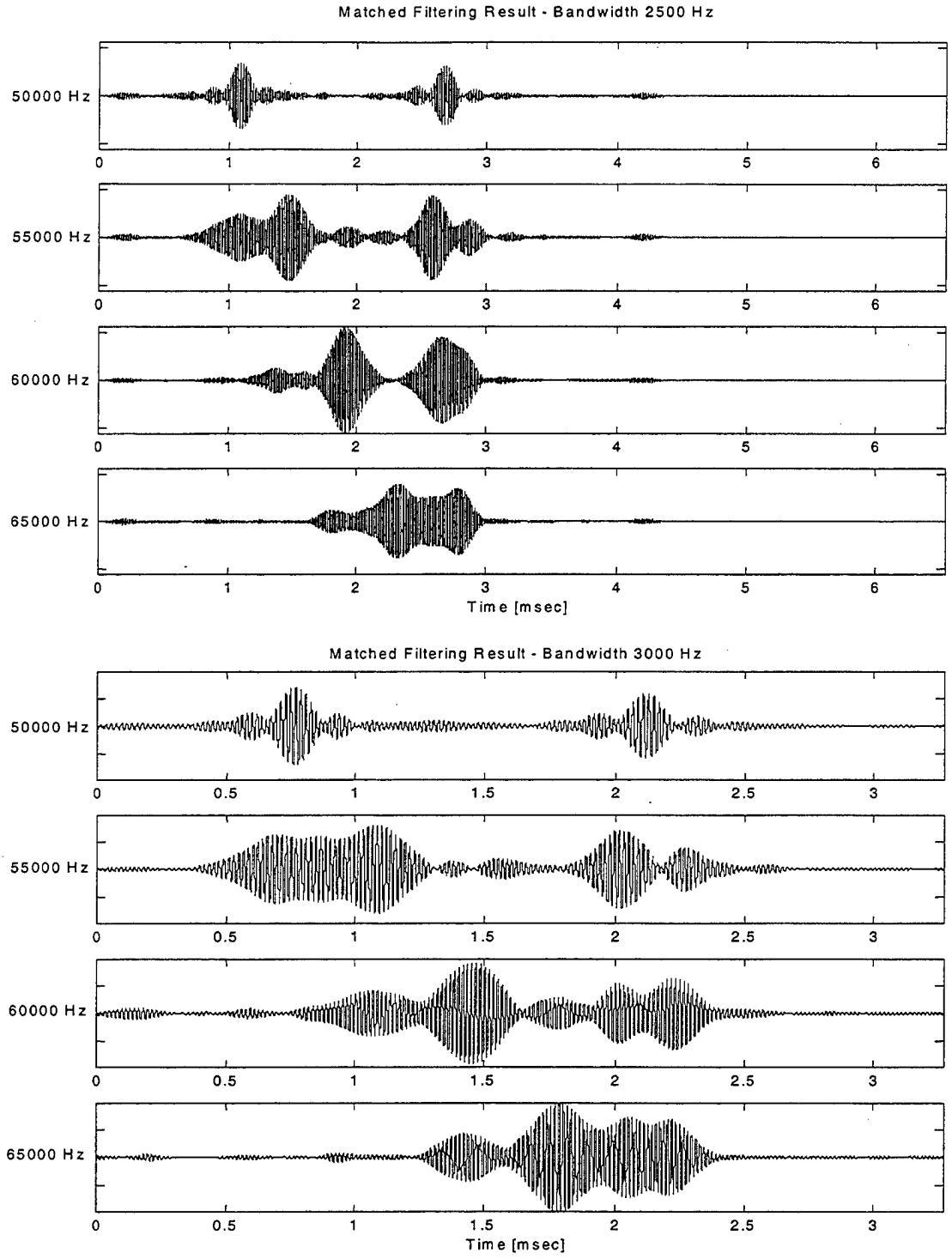

Figure 5.3. Two messages containing the symbols 1 - 2 - 4 – 8. The left message with a bandwidth of 2500 Hz is resolvable, the one on the right with 3000 Hz bandwidth is not resolvable.

B. FOCAL REGION SIZE

1. Full array

We used 2kHz bandwidth signals centered at 50 kHz and 65 kHz to determine the extent of the focal region. We found that the focal region has an ellipsoidal cross-section, with the major axis along the range direction and the minor axis along depth.

The extent in depth of the focal region is ± 1.5 cm as measured at the half-power point. This corresponds to a distance of about 0.6λ. The simulations for a frequency range of 400 Hz to 1200 Hz showed about 4λ focal region extend. Figure 5.4 shows the normalized, curve-fitted amplitude distribution over the depth for a signal that was sent from element two. The depth is shown relative to the intended focal position.

It can be seen that the energy distributions for both frequencies differ. The higher frequency has a stronger sidelobe. This is due to a higher attenuation of the higher modes contained in the higher frequency signal, which causes the sidelobes to become stronger. This is in contrast to the simulation results done at frequencies of 400 Hz to 1200 Hz, where the higher frequencies had the smaller focal region size. The focal point is shifted slightly for the two frequencies, where the higher frequency is shifted a bit downward and vice versa. Both frequencies show an increased amplitude at depths close to the rigid bottom. This is a phenomena to be expected near a rigid bottom and has no relation to the focal region.

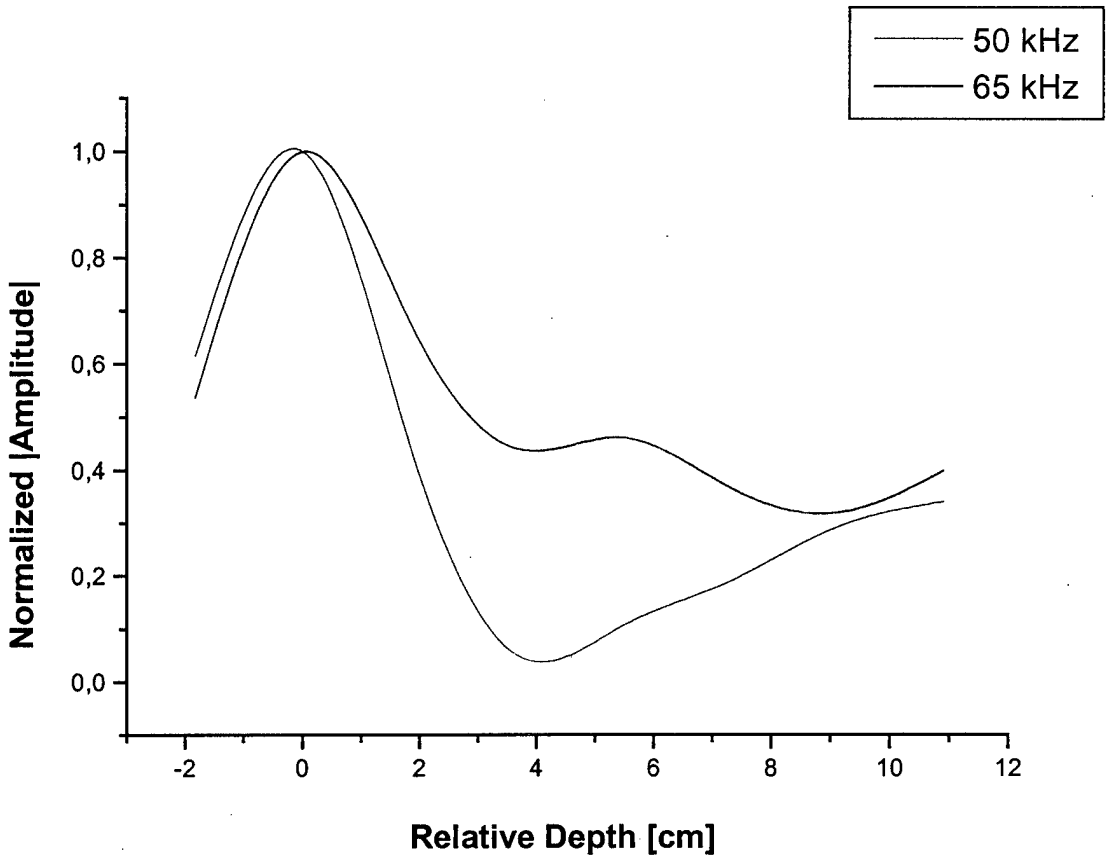

Figure 5.4. Focal region size in depth for a 50 kHz and a 65 kHz signal. The depth is measured relative to the intended focal point.

The extent in range of the focal region is much larger. For 50 kHz we found +9.5 cm and –8 cm at the half-power point. This is equivalent to about ± 3 wavelengths. The focal region for the 65 kHz signal extends +11 cm in direction of increasing range, slightly more than the 50 kHz signal. However, it is shifted in decreasing range by -5 cm and extends to -20 cm in the decreasing range direction. The equivalent wavelengths are about $+5\lambda$ and -9λ. Again the

simulations for a frequency range of 400 Hz to 1200 Hz showed a significantly larger extend.

The shifting and the sidelobe phenomena already noticed for the focal region along depth becomes more pronounced along range. The loss of energy and therefore information in the higher modes contained in the higher frequencies leads to a degradation of the focal region by a significant amount. The results are shown in Fig. 5.5.

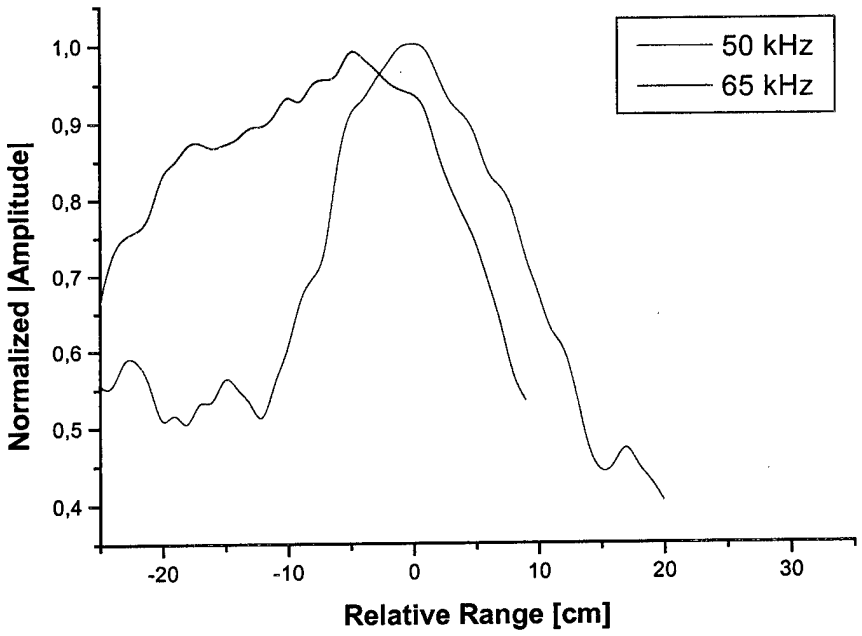

Figure 5.5. Focal region size in range for a 50 kHz and a 65 kHz signal. The range is measured relative to the intended focal point.

2. Focal region for 1 element

The response for one channel transmissions showed a weak focusing in space for most transmission channels as shown in Fig. 5.6. However, the time focus was still good for the intended focal point. It therefore can be concluded

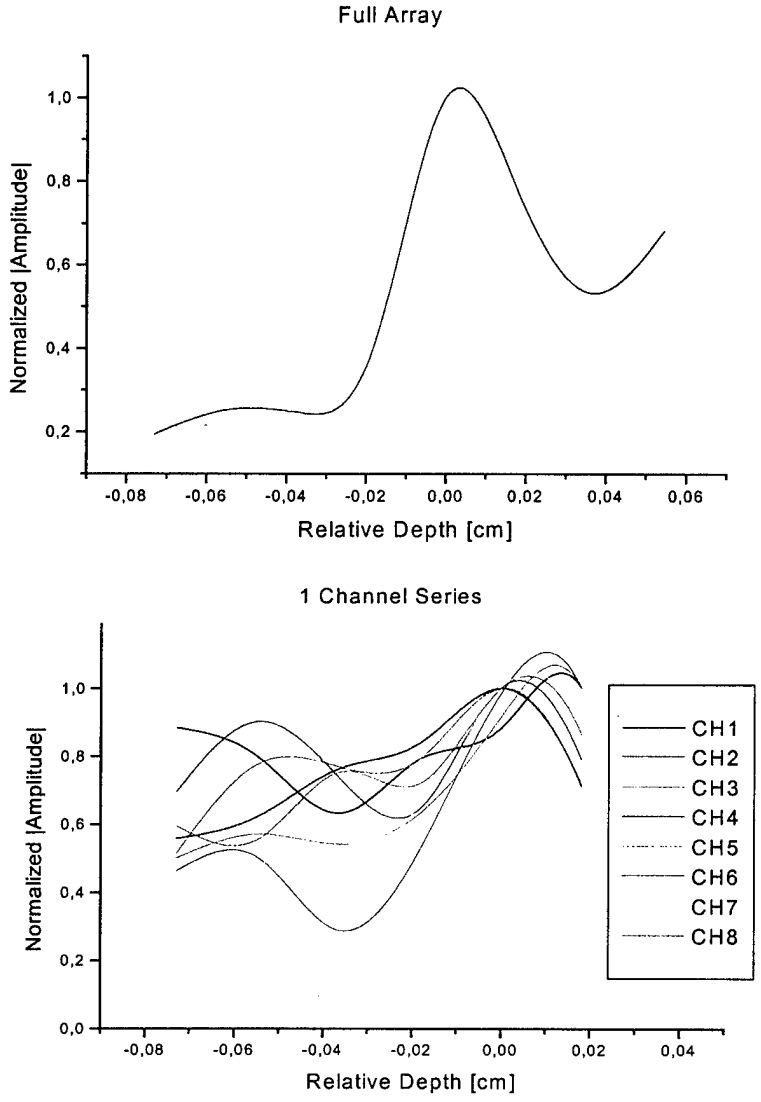

Figure 5.6. Focal region size in depth for a 50 kHz. The left side shows the full array response, the right side the response for one transmission channel for each of the eight channels. The depth is measured relative to the intended focal point.

that, if only a time focus is wanted, it is good enough to use a single element. The response will then be strongly dependent on location of the transmission. The closer the transmitting transducer is to a layer boundary, the surface or the bottom, the worse the response will be.

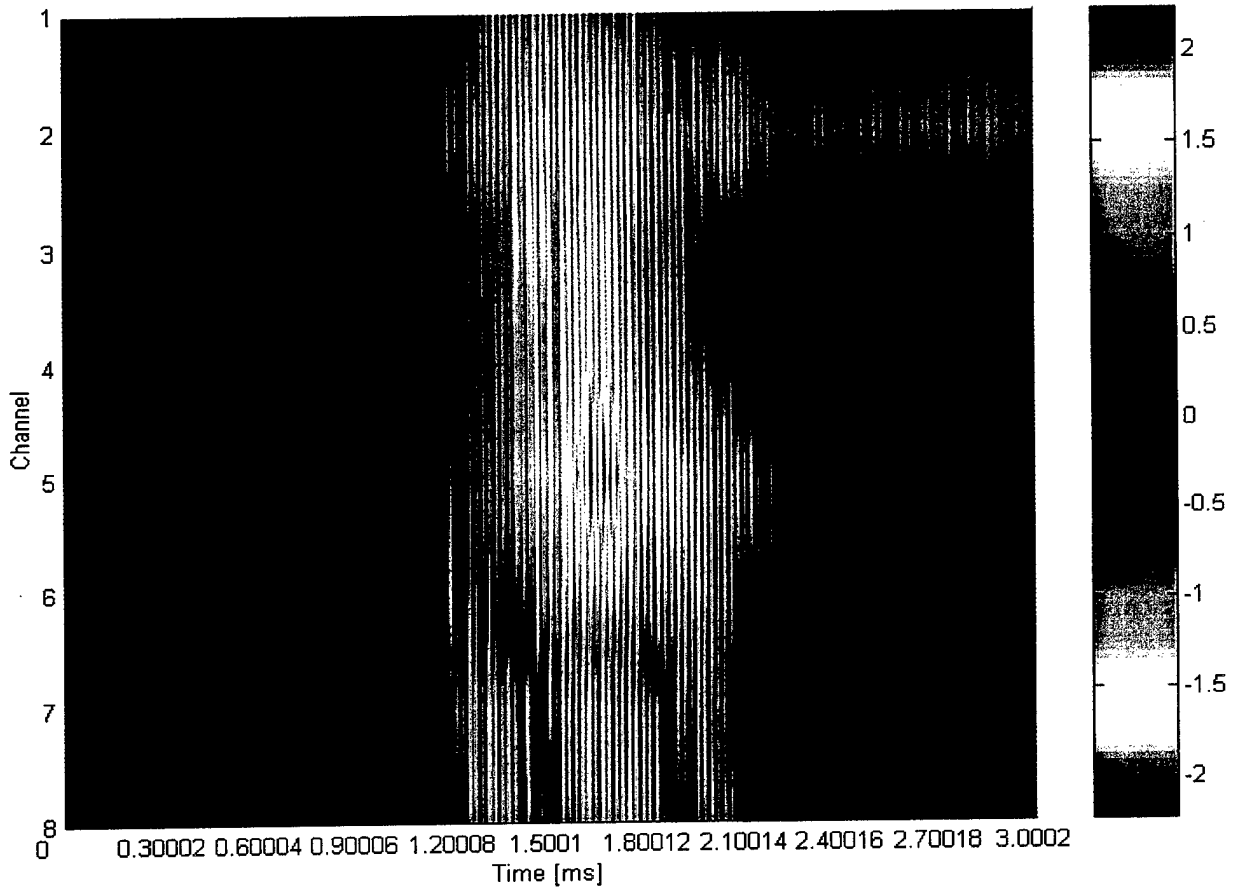

Figure 5.7. Time focus versus depth for a 50 kHz signal send only from channel 3. The energy is spread both in time and depth. However, for the intended focal point on channel five the time focusing is acceptable.

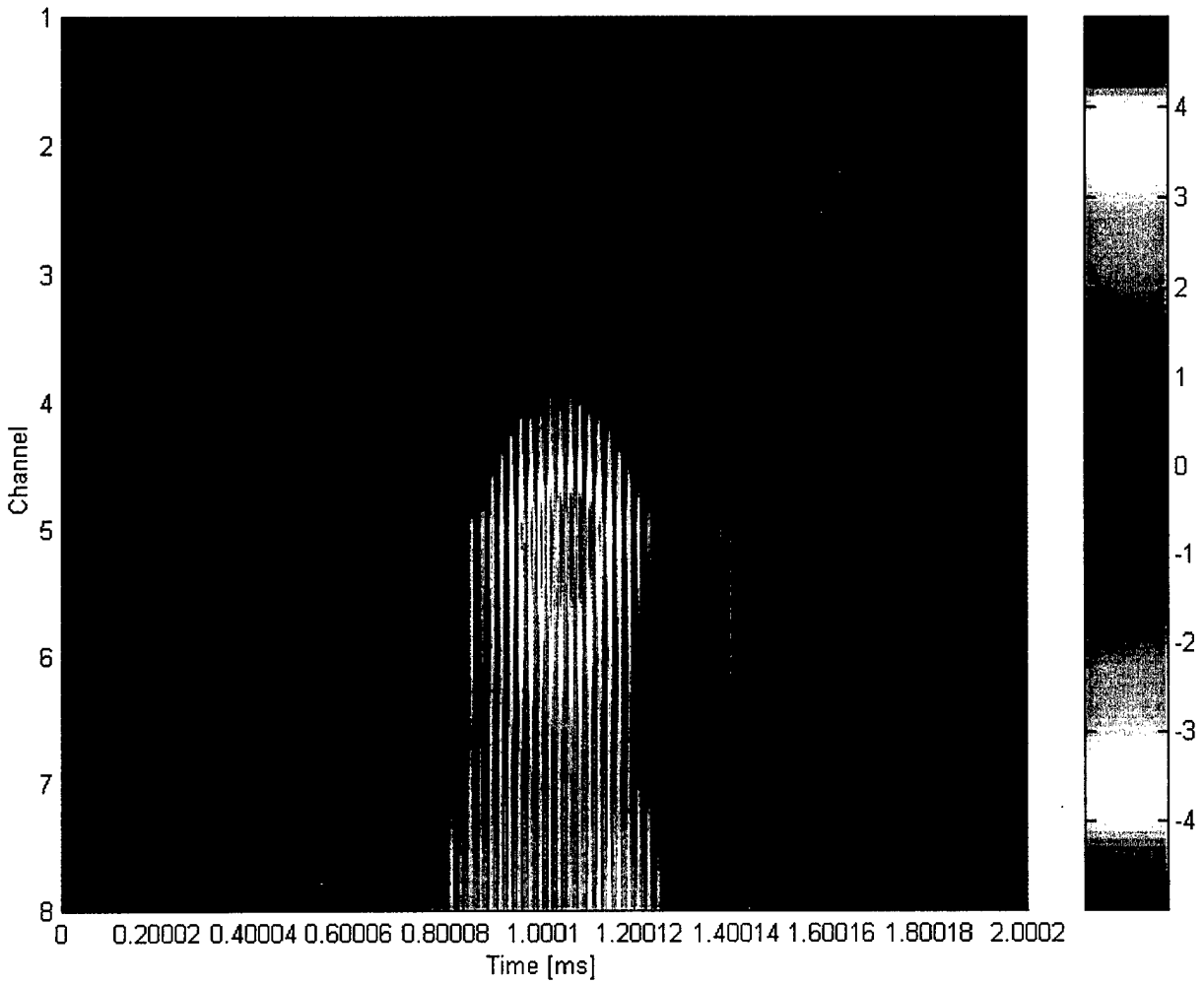

Figure 5.8. Time focus versus depth for a 50 kHz signal send from all channels. The energy is well focused on the intended focal point.

In Fig. 5.7 the intensity in time versus depth (channels) of a transmission from channel 3 is shown. This is to be compared to the response of the full array transmission as shown in Fig. 5.8.

3. Focal region for 2 elements

The response for two channel transmissions showed a significantly better focusing in space for most transmission channels, as shown in Fig. 5.9, than

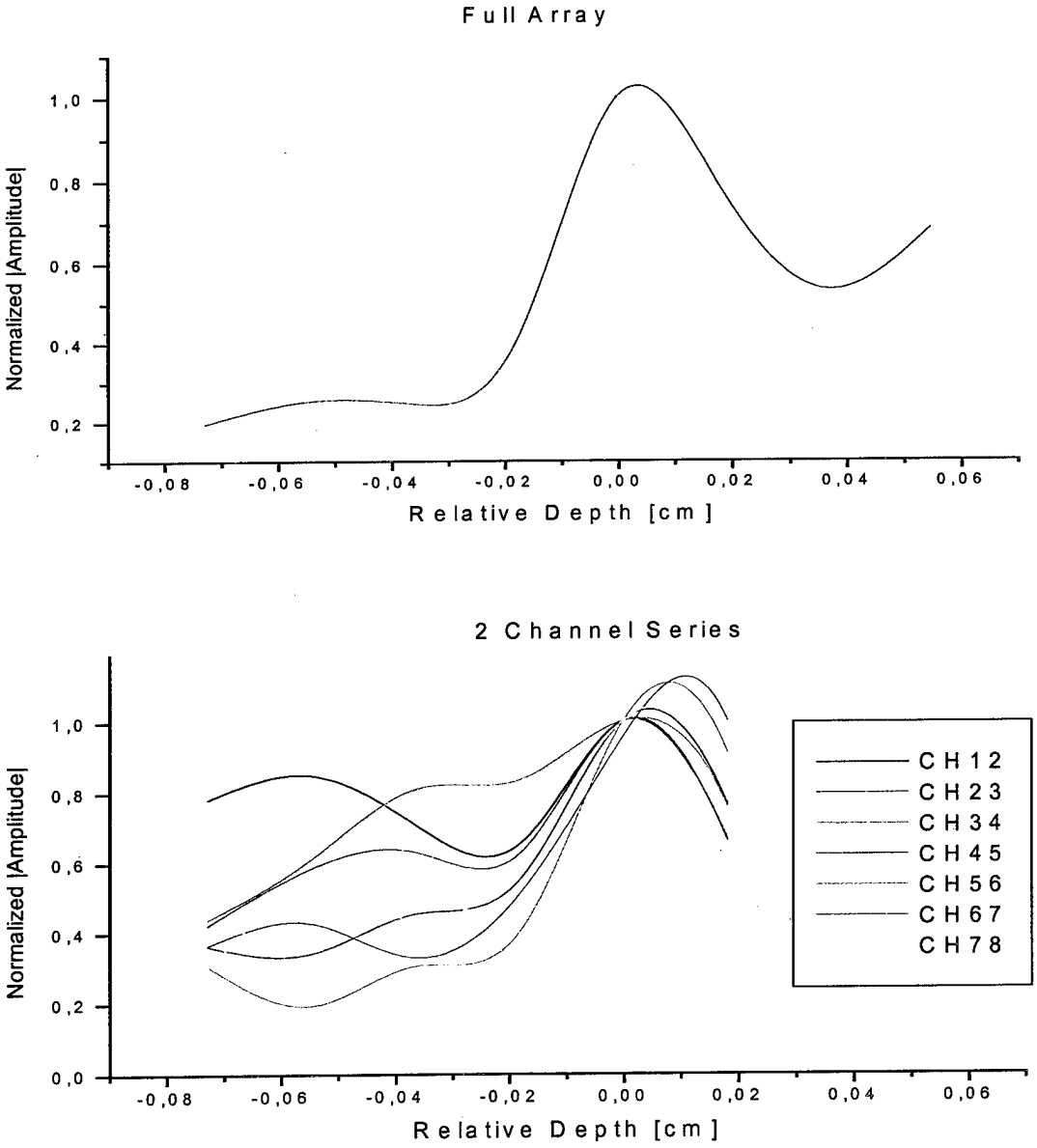

Figure 5.9. Focal region size in depth for a 50 kHz. The left side shows the full array response, the right side the response for two successive transmission channels for each of the seven possible combinations. The depth is measured relative to the intended focal point.

the 1 channel transmissions. The time focus was also better for the intended focal point as is shown in Fig. 5.10 (again compare to Fig. 5.8).

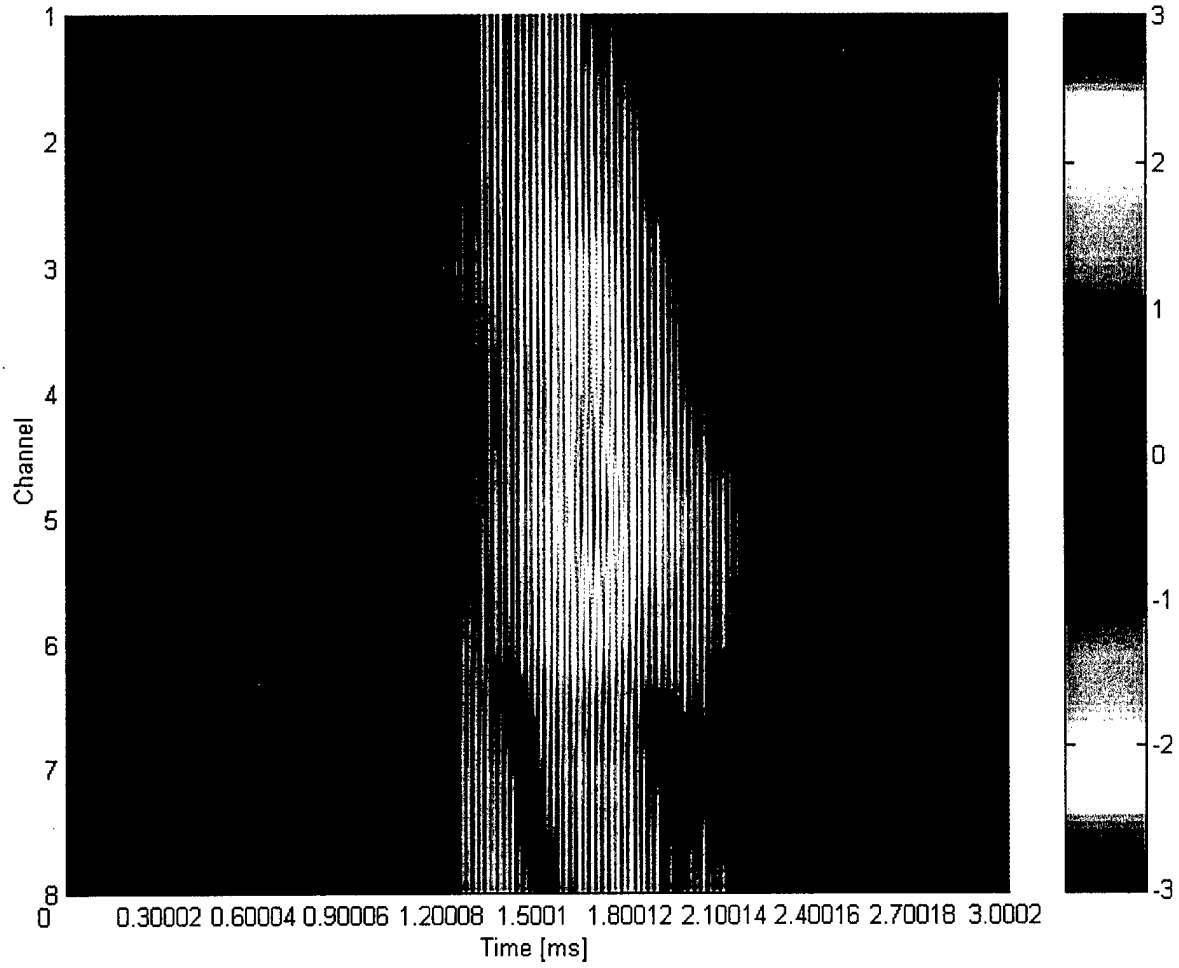

Figure 5.10. Time focus versus depth for a 50 kHz signal send from channel 3 and 4. The energy is spread both in time and depth. However, there is a good focus in time given for the intended focal point on channel five.

4. Focal region for 3 elements

The response for a three channel transmission showed a very good

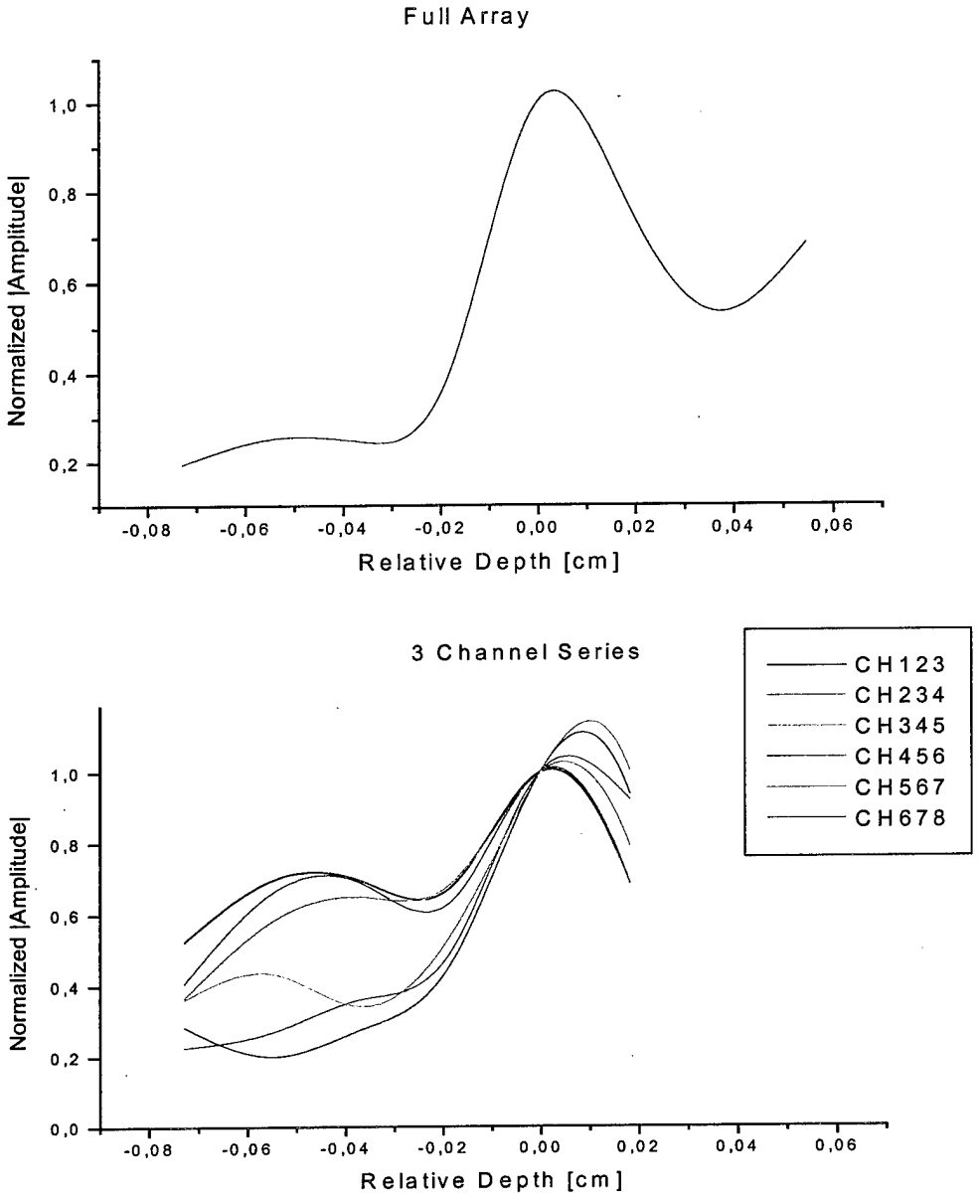

Figure 5.11. Focal region size in depth for a 50 kHz. The left side shows the full array response, the right side the response for three successive transmission channels for each of six possible combinations. The depth is measured relative to the intended focal point.

focusing for both time and space as can be seen in Fig. 5.11 and Fig. 5.12. This should be expected. The more elements of a vertical array used, the better will be the focusing. Thereby three array elements within a wavelength are commonly used to get good sampling. However, an array with two elements, arranged with a distance of less than a wavelength is sufficient, as we could show with our data.

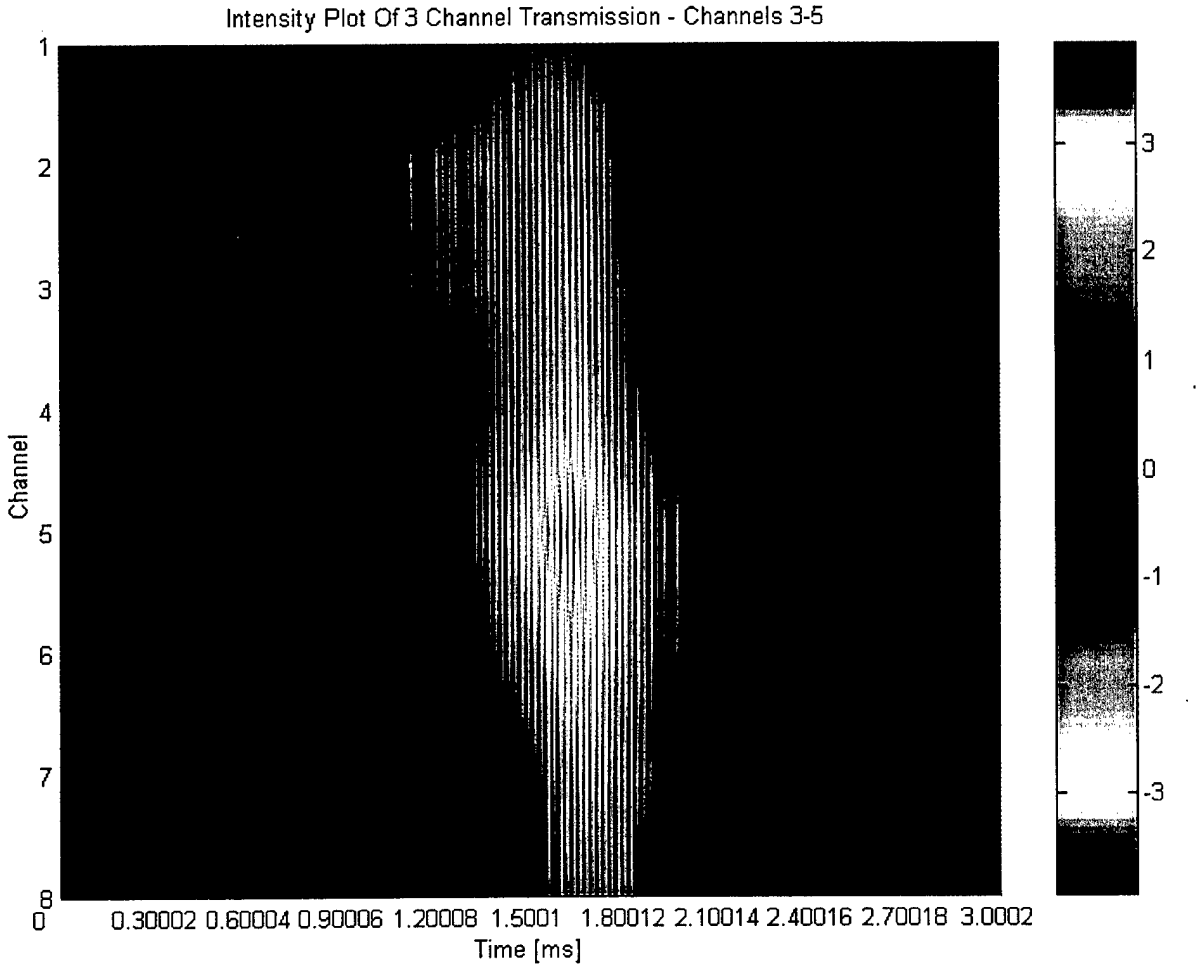

Figure 5.12. Time focus versus depth for a 50 kHz signal send from channel 3,4 and 5. The energy is spread in depth. There is a very good focus in time for the intended focal point on channel five and a satisfying time focus on the other channels.

C. FOCAL REGION STEERING IN RANGE

By shifting the frequency, the focal region shifts. The measurements for the shifted focal region showed that the simple waveguide we used has a value of $\beta = 1$. For the 50 kHz signal a shift in range of 20 cm is achieved by a frequency shift of 2500 Hz. The focal region extent was the same for both the unshifted and shifted signal as is shown in Fig. 5.13 and Fig. 5.14. We conclude that shifting the focal region by 5% in range does not significantly change the size of the focal region.

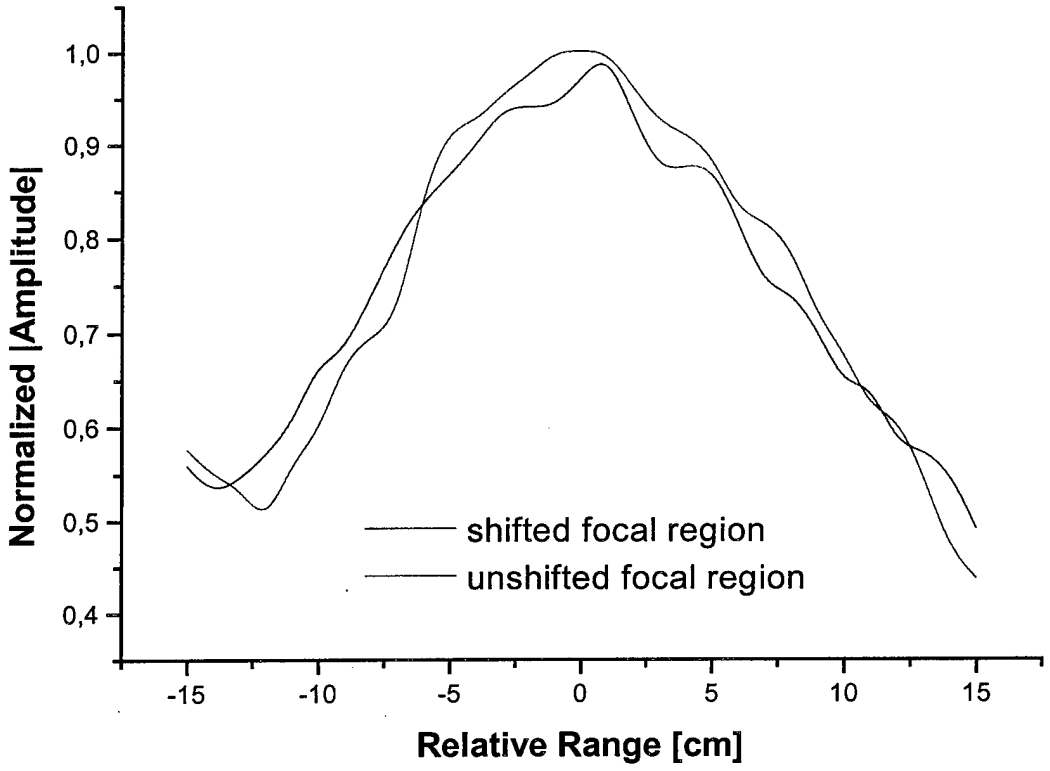

Figure 5.13. Focal region size in range of the unshifted and shifted signal. Both are measured and shown relative to the intended focal point.

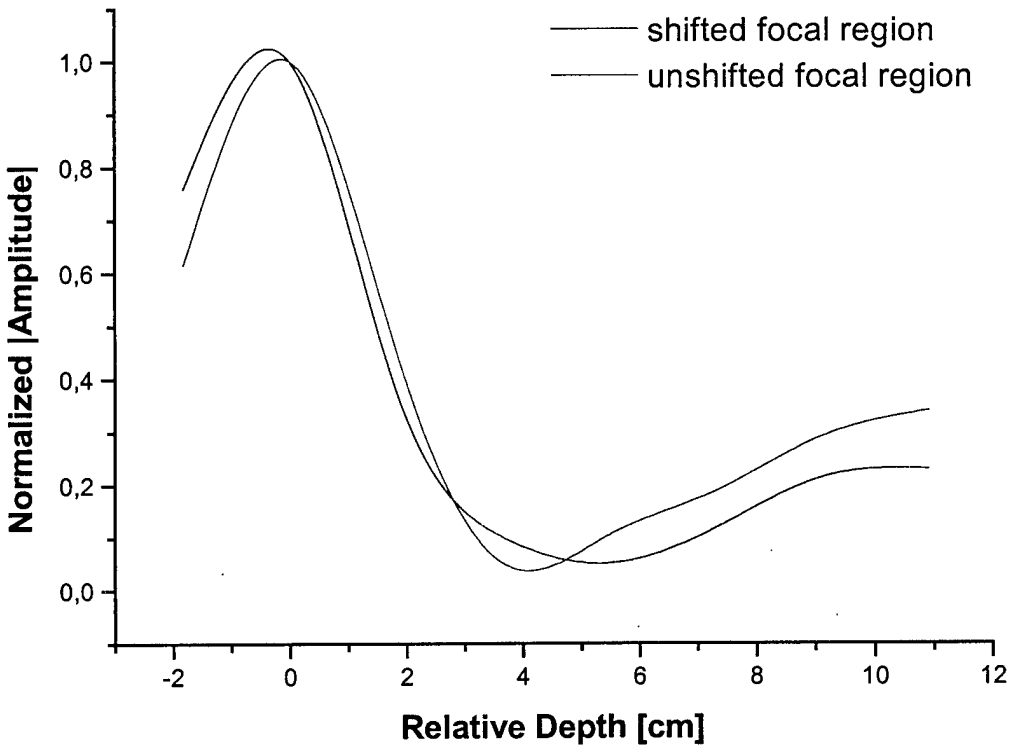

Figure 5.14. Focal region size in depth of the unshifted and shifted signal. Both are measured and shown relative to the intended focal point.

D. MESSAGES

Because the focal region is limited in size and there are strong sidelobes outside of that region, there is a natural encryption built into the transmission of messages. The signals do not focus well in time outside of the focal region and therefore there is inter-symbol interference that makes it impossible to recover

the messages. In order to prove this we defined a simple code using the 15 symbols we get from the 4 center-frequencies. This code is shown in Table 5.1.

General	
Symbol	**Meaning**
14	number follows
15	word follows
_(space)	shift for second half of letters

Numbers	
Symbol	**Meaning**
1	1
2	2
3	3
4	4
5	5
6	6
7	7
8	8
9	9
10	0
11	+
12	-
13	.

Letters	
Symbol	**Meaning**
1	A
2	B
3	C
4	D
5	E
6	F
7	G
8	H
9	I
10	J
11	K
12	L
13	M
_1	N
_2	O
_3	P
_4	Q
_5	R
_6	S
_7	T
_8	U
_9	V
_10	W
_11	X
_12	Y
_13	Z

Table 5.1. Simple code using 15 symbols.

1. Message at the intended reception point

The message we used was "DEC 99", which using the simple code above reads "15-4-5-3-14-9-9" in symbols. This message could clearly be read at the focal point using a matched filter analysis. Figure 5.14 shows the matched filter

result. Comparing this with the Table 5.2, in which the center-frequencies of the symbols transmitted are shown, shows that the message is correctly transmitted and easily resolved.

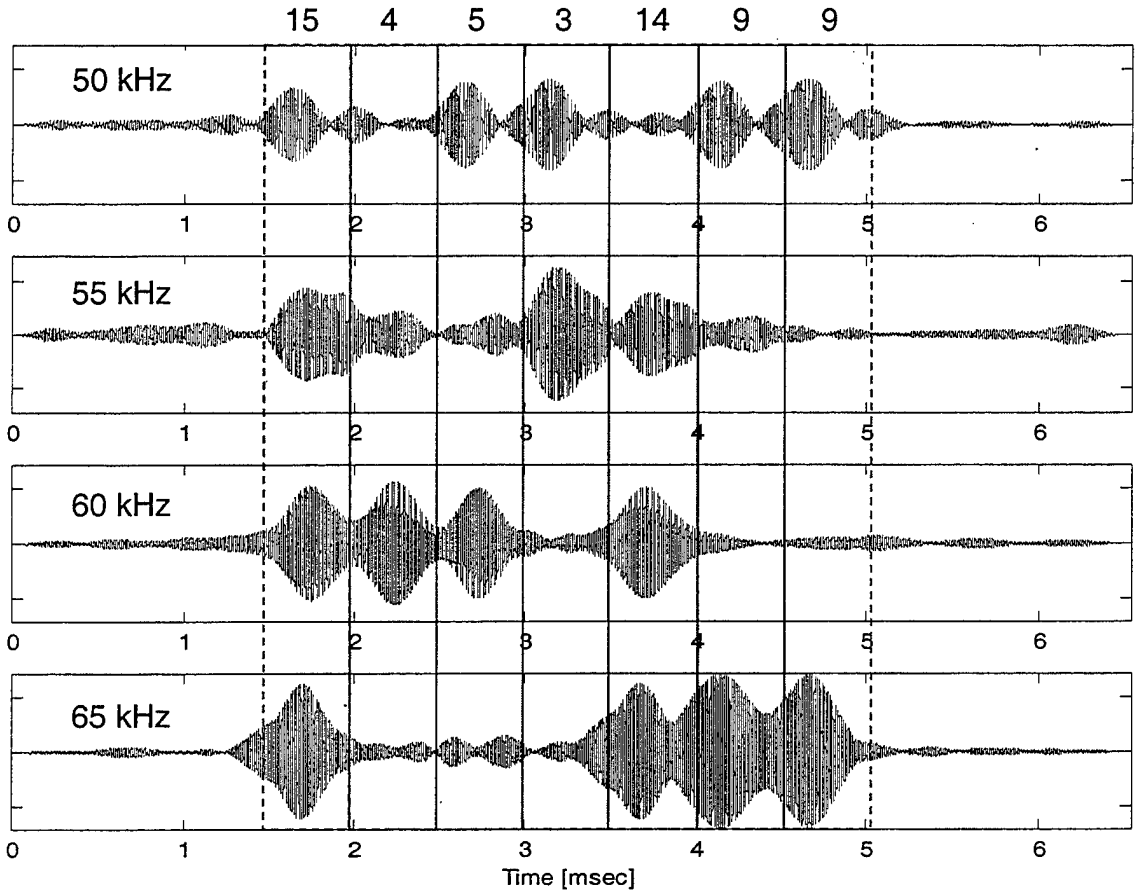

Figure 5.14. Matched-filter analysis of the incoming message. The message is clearly and easily resolvable. The red boxes show the symbols with respect to time.

Symbol	15	4	5	3	14	9	9
50 kHz	x		x	x		x	x
55 kHz	x			x	x		
60 kHz	x	x	x		x		
65 kHz	x				x	x	x

Table 5.2. Center-frequencies transmitted for the symbols of the message "DEC 99" using the simple code defined in Table 5.1.

2. Message outside the focal region

The message outside the focal region is naturally encrypted. This can be seen in Fig. 5.15, where the message from Table 5.2 is used again but is received outside the focal region.

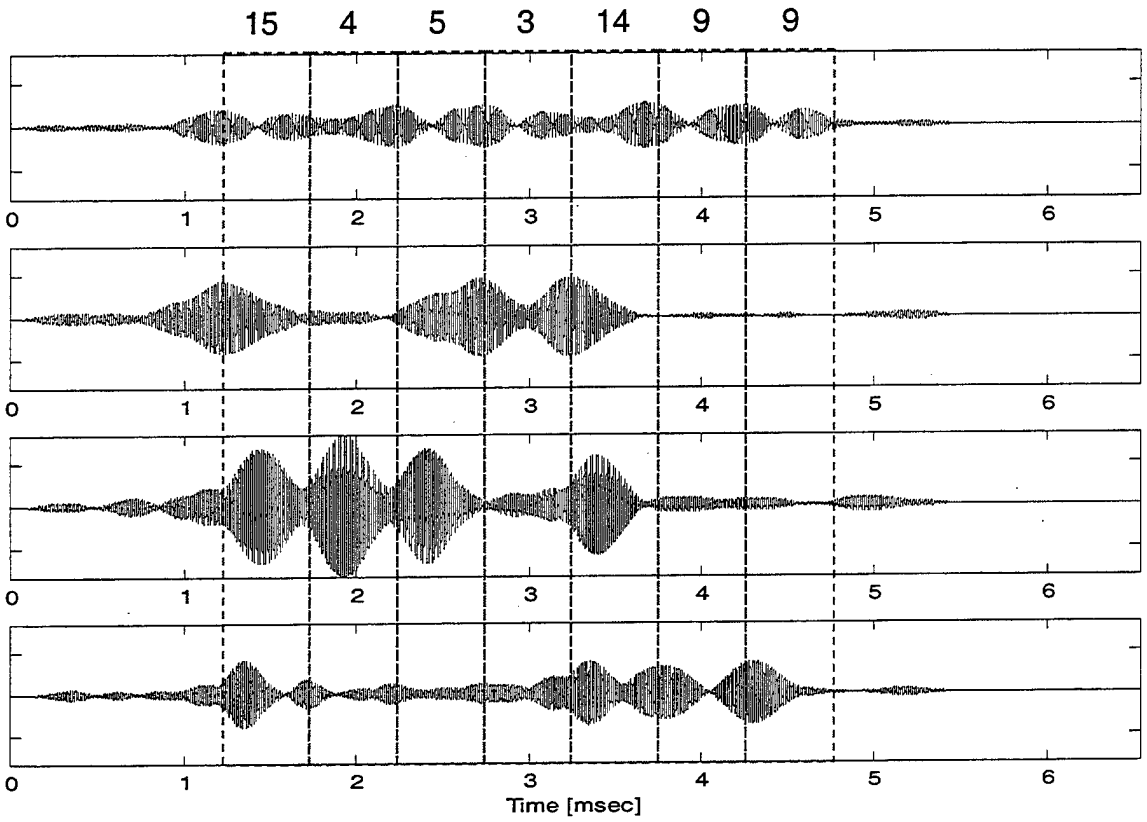

Figure 5.14. Matched-filter analysis of the incoming message outside the focal region. The message is unclear and not resolvable. The red boxes show the symbols with respect to time.

Symbol	14	4	4	2	14	10	8
50 kHz							
55 kHz	x			x	x	x	
60 kHz	x	x	x		x		
65 kHz	x				x	x	x

Table 5.3. Center-frequencies as received outside the focal region resulting in the symbols of a message reading "442 08" using the simple code defined in Table 5.1.

Note that for the higher frequencies the signal becomes clearer and easier to resolve. This is due to the higher attenuation of the higher modes of the partial pulse. The energy propagating on the direct path is less attenuated and therefore relative to the other paths is dominating. This reduces the effect of natural encryption. Also, it should be noted that the response of our system is less strong for the lower frequencies due to the frequency roll-off of the elements of the array.

For the message shown we used a bandwidth of 2000 Hz. This is equivalent to a data rate of 2000 symbols per second. Since the symbols we used where built from four center-frequencies we can also express that number as 8000 bits per second. We have shown earlier that the limit we could achieve with our system was a bandwidth of 2500 Hz. This is equivalent to a limit of 2500 symbols per second or 10000 bits per second.

THIS PAGE IS INTENTIONALLY LEFT BLANK

VI. CONCLUSIONS

A. CONCLUSIONS

In this thesis experimental studies were conducted to test results of analytical and numerical work on time-reversed signal underwater communication. The experimental results indicated a good basis for further experimental work both in scale model experiments and at-sea experiments.

The experimental results agree with earlier numerical work in regards to the focusing properties. That is, the size of the focal region is larger in range (horizontal) than it is in depth (vertical). The focal region size was found to be only a few wavelengths along the horizontal direction and less than one wavelength along the vertical direction. Outside the focal region intersymbol interference occurs due to the lack of time focusing, which provides a natural encryption property. This can be of advantage especially in military use. It also means that a vertical change of position is more critical to communication than a horizontal change.

We have also shown that the focal region can easily be shifted in range by frequency shifting of the time-reversed signal. If a planar array is used, a shift in the bearing angle can be achieved with commonly used beamforming techniques. Thus, the location of the focal region can be adjusted to stay at the position of a moving receiver, such as an autonomous underwater vehicle or submarine.

Experiential results also show that there is an optimal value for the relation between bandwidth and spacing of center-frequencies. For 5 kHz center-frequency spacing the optimal bandwidth was found to be to be 2.5 kHz. Thus, a total bandwidth of 10000 Hz is needed to transmit a data rate of 10000 bits per second. These results show that the TRA approach offers powerful means for high data rate underwater communication because of reduced inter-symbol interference and bandwidth efficiency.

A problem arising from the stronger attenuation of higher modes of the time-reversed signal is the degradation in spatial focusing. The time focusing was however not affected from this attenuation.

The spatial focusing properties depend on the aperture size and number of elements per wavelength. This work showed a slight improvement in the spatial side-lobe amplitude for the use of a larger aperture while keeping the element spacing constant. The degradation of the focal region with less aperture size and therefore less number of elements is due to reduced spatial sampling as well as less energy transmitted. However, focusing in time still occurred, indicating that the necessity of guard times with a time-reversal approach can be eliminated.

B. RECOMMENDATIONS FOR FURTHER EXPERIMENTS

Steering the focal region could only be investigated for a range shift. However, a shift in relative depth needs to be investigated. In general, depth shifting of the focal region can be done by shifting the relative phase between the

elements of the array. Note that the phase shift has to be applied to a signal containing multimode information, making this a very involved and difficult process.

Further efforts should be made in investigating the application of other communication approaches in order to combine them and thereby increase the data rate. For example, the use of different phase information for a fixed center frequency might be a way to combine the algorithm and increase the data rate.

Before this approach can be implemented in a real system, it is necessary to prove the reliability in real environments. A step in that direction could be to add noise in a simple environment like our tank and to increase the complexity of our environment.

Finally, a very interesting and instructive area of research is to perform benchmark testing of different communication schemes and determine their limitations and advantages over the TRA technique. A group of researchers at the Naval Postgraduate School is already embarking on such a task.

THIS PAGE IS INTENTIONALLY LEFT BLANK

LIST OF REFERENCES

Abrantes, A.A.M., Smith, K.B., and Larraza, A., **(1999)**. "Examination of time-reversal acoustics and applications to underwater communications", *Journal of the Acoustical Society of America*, Vol. 105, pp. 1364

A&T Engineering Technologies, VECTOR Research Division, "Acoustical Materials Engineering"

EDO Corporation, Acoustic Division, **(1998)**, "Calibration Reports Serial # 5815-001/002"

Fink, M., **(1997)**, "Time Reversed Acoustics", Physics Today, March 1997, pp. 34-40

Gage Applied Sciences Inc., **(1998)**, "CompuGen 1100 - Hardware Manual and Installation Guide", 2nd Ed.

Gage Applied Sciences Inc., **(1998)**, "CompuScope 512 - Hardware Manual and Installation Guide", 1st Ed.

Jackson, D. R. and Dowling, D.R., **(1991)**, "Phase conjugation in underwater acoustics", *Journal of the Acoustical Society of America*, Vol. 89, pt. 1, pp. 171-181

Jensen, F.B., Kuperman, W.A., Porter, M.B., Schmidt, H., **(1993)**, "Computational Ocean Acoustics", *American Institute of Physics*

Kuperman, W. A., Hodgkiss, W.S., Song, H.C., Akal, T., Ferla, C., Jackson, D.R., **(1998)**, "Phase conjugation in the ocean: Experimental demonstration of an acoustic time-reversal mirror", *Journal of the Acoustical Society of America*, Vol. 103, pt. 1, pp. 25-40

Smith, K.B., Abrantes, A.A.M. and Larraza, A., **(1999)**, "Examination of time-reversal acosutics in shallow water and applications to noncoherent underwater acoustic communications." Submitted to the *Journal of the Acoustical Society of America*

Song, H.C., Kuperman, W.A., Hodgkiss, W.S., **(1998)**, " A time-reversal mirror with variable range focusing", *Journal of the Acoustical Society of America*, Vol. 103, pt. 6, pp. 3234-3240

INITIAL DISTRIBUTION LIST

1. Defense Technical Information Center.....2
   8725 John J. Kingman Rd., STE 0944
   Ft. Belvoir, VA 22060-6218

2. Dudley Knox Library.....2
   Naval Postgraduate School
   411 Dyer Rd.
   Monterey, CA 93943-5101

3. Prof. A. Larraza, Code PH/La.....4
   Department of Physics
   Naval Postgraduate School
   Monterey, CA 93943-5002

4. Prof. K.B. Smith, Code PH/Sk.....4
   Department of Physics
   Naval Postgraduate School
   Monterey, CA 93943-5002

5. Prof. W. Maier, Code PH/Mw.....2
   Department of Physics
   Naval Postgraduate School
   Monterey, CA 93943-5002

6. KptLt M.G. Heinemann.....2
   Sophienhöh2
   D 24340 Eckernförde
   GERMANY